PAPER

Development progress of coating first wall components with functionally graded W/EUROFER layers on laboratory scale

View the article online for updates and enhancements.

Development progress of coating first wall components with functionally graded W/EUROFER layers on laboratory scale

Thomas Emmerich[1,a] , **Dandan Qu**[1]**, Bradut-Eugen Ghidersa**[2] **, Martin Lux**[2]**, Jörg Rey**[2]**, Robert Vaßen**[3] **and Jarir Aktaa**[1]

[1] Karlsruhe Institute of Technology (KIT), Institute for Applied Materials, Hermann-von-Helmholtz-Platz 1, Eggenstein-Leopoldshafen 76344, Germany
[2] Karlsruhe Institute of Technology (KIT), Institute of Neutron Physics and Reactor Technology, Hermann-von-Helmholtz-Platz 1, Eggenstein-Leopoldshafen 76344, Germany
[3] Forschungszentrum Jülich GmbH (FZJ), Institute of Energy and Climate Research, Wilhelm-Johnen-Straße, Jülich 52425, Germany

E-mail: mv3058@partner.kit.edu

Abstract

In the course of developing functionally graded tungsten/steel-layer systems as protective coatings for the first wall (FW) of future fusion reactors, an overview of the results attained so far is given. This includes the determined parameters for creating such systems by vacuum plasma spraying on a laboratory scale and the achieved material properties determined in previous works. To realize the coating of future full scale FWs as well, the coating process is adapted to larger coating areas in the form of mock-ups. For such components, special attention needs to be paid to the challenges of the limited temperature window during coating to achieve good coating adhesion, whilst avoiding exceeding the tempering temperature of the steel. One successfully coated mock-up is also exposed to fusion-relevant heat loads in HELOKA (Helium Loop Karlsruhe) to evaluate the coating system behavior and verify its durability. Finally, for even larger components the coating design and process are further optimized, supported by finite element simulations.

Keywords: tungsten, first wall, functionally graded material (FGM), vacuum plasma spraying, finite element simulation

(Some figures may appear in colour only in the online journal)
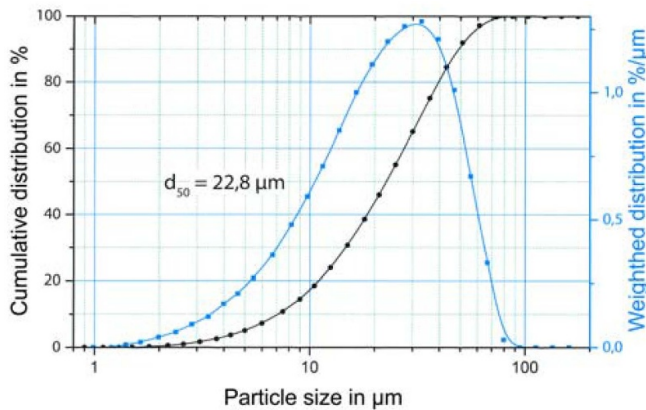
1. Introduction

For the first wall (FW) breeding blankets of future fusion power plants, it is envisaged to protect the steel structures against the plasma using tungsten (W)-coating, because of its favorable thermo-mechanical properties and low sputtering yield. Functionally graded (FG)-layers between the W-coating and the steel substrate, e.g. the reduced activation ferritic martensitic (FM) steel EUROFER, compensate for the difference in the coefficient of thermal expansion (CTE) [1].

In collaboration with the IEK-1 of Forschungszentrum Jülich [2] several batches of such layer systems were successfully produced [3–5] on a laboratory scale using the vacuum plasma spraying (VPS) technique. The layer systems were tested in regard to their mechanical and thermal properties and an overview of the results is given in this paper, together with the experimentally determined and utilized spraying

---

[a] Author to whom any correspondence should be addressed.

Figure 1. Particle size distribution of the steel powder.

Table 1. Average steel-powder composition in mass-%.

C	N	O	V	Cr	Mn	Fe	Ta	W
0.090	0.004	0.056	0.199	8.730	0.396	Bal.	0.059	1.081

parameters. Following the process development towards the future of coating, large scale FW is presented. As a first step, two representative FW mock-ups were produced, coated and inspected by nondestructive methods. One of these mock-ups was also tested under fusion-relevant heat loads and helium (He)-coolant flows to evaluate the durability of the coatings. Finally, another larger mock-up was produced and also successfully coated after optimization of the coating, supported by finite element (FE)-simulations.

2. Production of FG W/EUROFER coatings

2.1. Spraying powder and process parameters

In this section, an overview of the powder and spraying parameters used for producing the layer systems on a laboratory scale is given. In regard to the coating materials, stock W-powder AW3105 from the company Eurotungstene is used with, according to its datasheet, a guaranteed W-content of at least 99.86 mass-% and a mean particle size of about 12 μm. EUROFER-powder was procured from the company Nanoval, and produced by mixing the parent materials in a melt, aiming for the target composition of EUROFER [6], then sprayed in argon (Ar) in a way to achieve the chosen maximum particle diameter (D90 = 52 μm) and thus a mean particle diameter of about 23 μm (figure 1).

Specifically for the coating of the mock-ups, the composition of the received powder was controlled by chemical analysis, in particular inductive coupled plasma optical emission spectroscopy, combustion analysis and carrier gas hot extraction, of which the average values are listed in table 1. Compared to the target composition of EUROFER [6] the tantalum (Ta)- and the nitrogen (N)-content are lower, whereas the oxygen (O)-content is higher than specified. The standard deviation amounts to 0.1 mass-% for the parent element iron (Fe) and generally to less than 0.02 mass-% for the alloying elements.

Deposition on laboratory scale was performed at Forschungszentrum Jülich in a VPS unit from Oerlikon Metco, Switzerland, using the plasma gun F4. Table 2 lists the optimized coating process parameters [2], also taken for coating in

this work. The metal powders are injected separately into the plasma by two internal injectors inside the equipped nozzle (8 mm diameter). Both injectors are located at the bottom of the nozzle, at an angle of 45° to each other, to align the trajectory of the powders in the plasma plume and ensure homogenous material distribution on the substrate [2].

The feeding rates of EUROFER- and W-powder for 100% EUROFER and 100% W coatings are in the range of 28 g min^{-1} and 55 g min^{-1}, respectively [2]. By varying the feeding rate of both powders, the functional gradation is created.

The greatest challenge during the coating of EUROFER, and generally ferritic martensitic steels, is maintaining the components within a specific temperature window, as will be shown in detail below. On the one hand the substrate temperature should not be too low, to ensure the adhesion of the coating, and on the other hand the temperature should not exceed the substrate tempering temperature either, as otherwise the material strength decreases. To cope with the latter, the plasma plume is regularly moved from the sample, allowing the substrate to cool down before it reaches its tempering temperature. Furthermore, coating can also be conducted with a faster spraying system movement speed of 0.5 m s^{-1}, which moderates the loss of material hardness [4] without affecting the layer adhesion significantly [7]. The faster movement shortens the local contact time between the plasma plume and the substrate and thus reduces the amount of heat the sample surface receives, so that the substrate does not reach its tempering temperature so fast. Control of the coating process can be further improved, when suitable online monitoring of the internal temperature of the substrate is available, e.g. by the thermocouples implemented in the mock-ups (see also section 3).

2.2. Overview of preceding development and achieved layer properties

First, FG W/EUROFER VPS-coatings, which had been created in a previous project for divertor application [8, 9], were deposited on Ø 10 mm cylindrical samples of a W/W-alloy substrate with a thickness of up to 1 mm and three gradation steps. These layer systems were tested in regard to their high temperature stability and it was shown that for the test time of 60 min the upper temperature limit can be extended up to 800 °C, because the precipitation of Fe$_2$W intermetallic compounds (IMC) starts at about 900 °C [9].

In view of the FW protection, coatings with three- and five-step FG-layers as well as a W-top coat were successfully deposited on 100 × 100 mm² large substrates made of the anticipated FW material EUROFER [3, 5]. The total FG-layer thickness was in the range of 300 μm to 700 μm, while the W-top coat had a nominal thickness of 500 μm [3, 5]. The actual total thickness was generally thicker than the specified

Table 2. VPS process parameters for W- and FG W/EUROFER-coatings [2].

	Current in A	Power in kW	Spraying distance in m	Argon volume flow in slpm	Hydrogen volume flow in slpm	Chamber pressure in mbar	Spraying system relative speed in m s^{-1}
Normal speed	680–750	50–51	0.3	40	11.5	60	0.44
Faster speed							0.5

one, with deviations in the range of 50 to 200 μm [3, 5]. The interfaces between the coating and substrate, as well as between the FG-layers themselves, were sound, without cracks or delaminations. The observed porosity of the W-top coat was generally below 5% [3, 5]. From these layer systems 50 $\times$ 10 mm^2 large pieces were cut and tested under edge-localized-mode (ELM)-like thermal shock loads, using the electron beam facility JUDITH 1 at FZJ. The samples withstood at least 100 single pulses at 0.19 GW m^{-2} with a duration of 1 ms and a 2 s pause in between, to allow the samples to cool down completely [3, 4]. Furthermore, the layer systems also showed no damage in the form of cylindrical samples of Ø 5 $\times$ 20 mm after 500 cycles of thermal fatigue between 350 °C and 550 °C in a vacuum furnace [3, 4]. Finally, at 550 °C satisfactory layer adhesion was determined by fracture mechanical bending tests, while the fracture surfaces showed indications of metallurgical bonding [3].

Thicker layer systems with 1.2 mm thick FG-layers and 0.8 mm thick W-top coats were also successfully created on 50 $\times$ 50 mm^2 large EUROFER substrates [3, 4], and thus the desired thickness of 2 mm for the W-coatings was achieved. A FG-layer thickness of 1.2 mm or higher is preferred, because FE-simulations indicate that then the maximum creep strain per thermal cycle in the EUROFER substrate decreases significantly [1]. Fracture mechanical bending tests on these layer systems showed interface toughness values similar to the former layer systems and also indications of metallurgical bonding [7]. These layer systems were also tested in regard to thermal fatigue, between 300 °C and 550 °C for up to 5000 cycles, and exhibited neither deterioration of the coating itself nor of the coating/substrate interface [10].

During the process development of coating the FW mock-ups, with internal cooling channels and coating areas of 270 $\times$ 65 mm^2 and larger, the unsuccessful coatings detached, as shown later. From these coatings Ø 12 mm disks were cut from random locations by electrical discharge machining (EDM) and the thermal diffusivity in the thickness direction was measured by laser flash. For the specific values of the four samples tested, each two for the pure W-top coat and for the complete 2 mm thick layer system, are plotted in figure 2(*a*).

Several data points have good congruency to each other, as their deviation is less than 5%, which is indicated by the error bars. In comparison to the literature data of W [11], the average measured values of the produced W-coatings are closer to the literature values of bulk- than to other VPS-W (figure 2(*b*)), which corroborates the use of the former data in previous works [7]. The higher agreement with the bulk-W values could be due to the comparatively lower porosity achieved during production. In comparison to EUROFER [12] (figure 2(*c*)) the coating exhibits a slightly higher thermal diffusivity, likely

due to the contribution of a more conductive tungsten phase whose volume fraction varies through the thickness and is in the lowermost layer, with 25 vol-% W nominally the lowest.

3. Production and testing of FW mock-ups

3.1. Production of FWI mock-ups

Due to the encouraging results obtained for small-scale material samples and in view of the real size blanket FW, it is of interest, first of all, whether coatings of similar quality and properties can also be deposited on substrates with larger surface areas and, particularly, with internal structures; secondly how such layer systems behave under conditions comparable to future fusion reactors.

Two mock-ups were fabricated out of 300 $\times$ 100 $\times$ 20 mm^3 large EUROFER plates with three cooling channels cut into the plates by EDM. Each channel has a rectangular cross-section of 10 $\times$ 15 mm^2 with a 2 mm filet radius (figure 3). The wall thickness between the channels and that between the channels and the top surface of the plate are 5 and 4 mm, respectively. In one of the walls separating the two channels, a Ø 1.5 mm hole was drilled from the backside of the plate to insert thermocouples. The hole has a depth of 18 mm, allowing temperature measurements inside the substrate up to a distance of 2 mm from the surface of the plate. Also first, simple manifolds made of EUROFER were welded to both ends of the mock-up by the tungsten inert gas (TIG)-technique. After welding, the mock-ups were heat treated with austenitization at 1050 °C for about 90 min, cooled to 170 °C and annealed at 760 °C for about 90 min. The welding and heat treatment parameters followed the procedures and guidelines for the FM-steel 1.4901 (P92) [13]. For fixing the mock-up in the holding frame during VPS, bores were drilled into the plate sides. Three of these four fixing points allow free movement in length and width, to avoid constraint stresses during coating. The coating, consisting of a 1.2 mm thick FG-layer and a 0.8 mm thick W-top coat, was sprayed onto the central part of the plate above the cooling channels on an area of 270 $\times$ 65 mm^2. A cover plate protected the rest of the mock-up, especially the welding seams and the holding frame, against the spraying.

VPS was performed at Forschungszentrum Jülich with one mock-up coated with normal speed and the other with faster robot speed (table 2). The latter was tested specifically, because the cooling channels reduce the amount of material for heat transfer in the central area, so that local overheating and loss of the material strength of the substrate could be possible. Preheating of the plate was achieved by a plasma plume

a

b

c
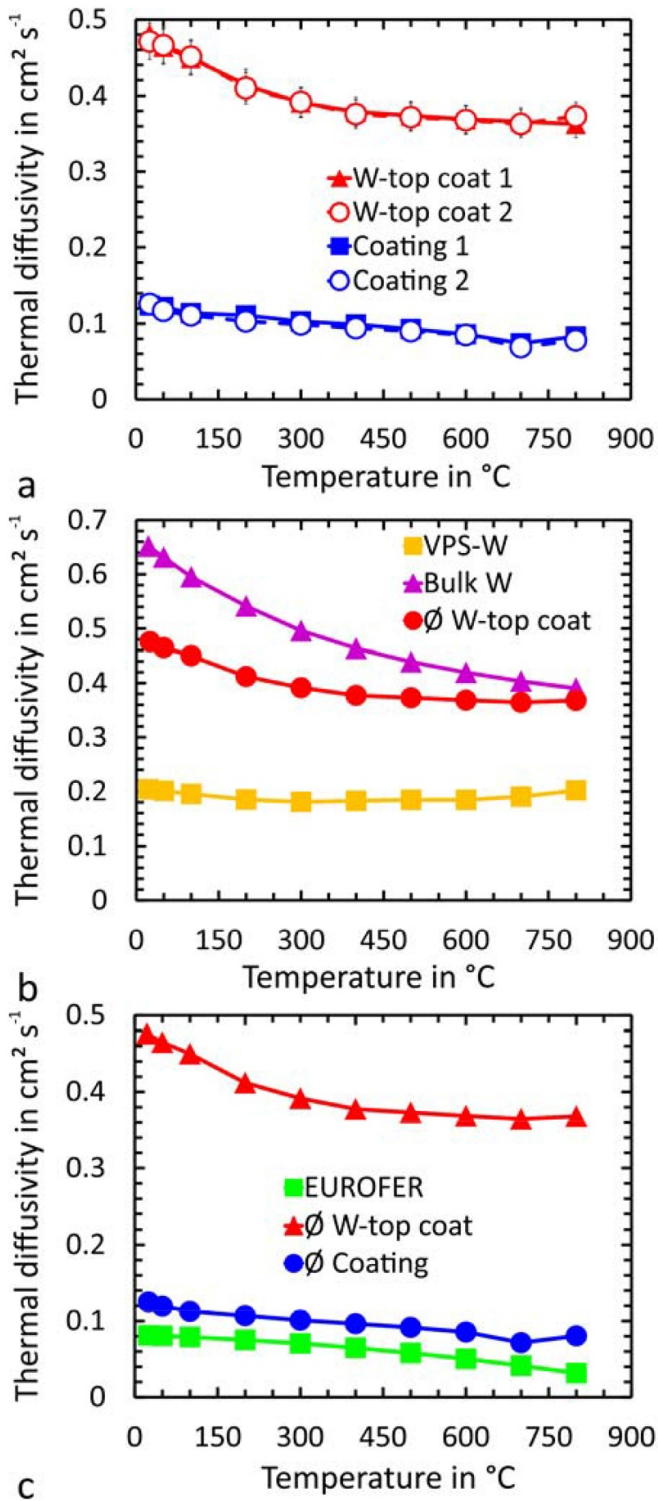
Figure 2. Measured thermal diffusivity and comparison of (*a*) the individual samples to each other, (*b*) the mean measured value of the W-top coat to the literature data of W [11] and (*c*) the measured values to the literature data of EUROFER [12].
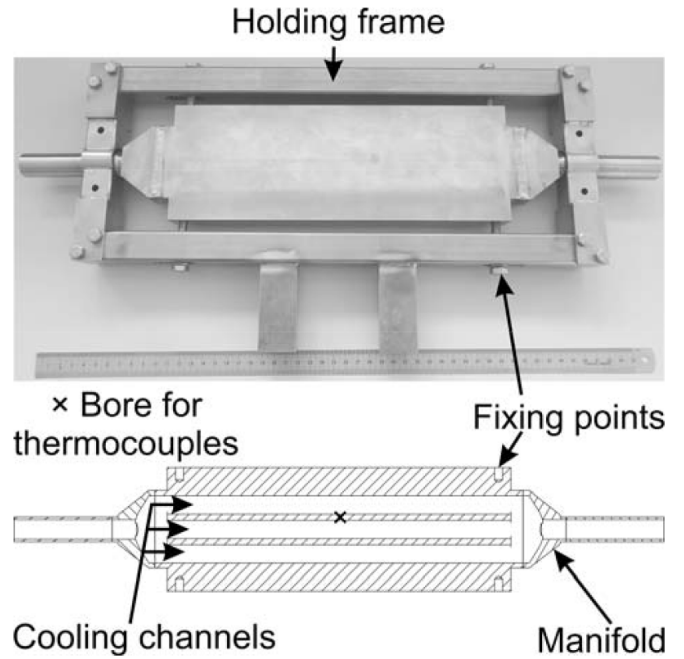
Figure 3. Mock-up after welding, fixed to its holding frame, and its schematic cross-section.

The temperature trends measured by the thermocouples during spraying at normal speed are plotted in figure 4 and for spraying with faster robot speed in figure 5. During spraying using normal speed (figure 4) the maximum temperatures are near, but mainly below the annealing temperature of the material of 760 °C. Cooling was achieved by removing regularly the plasma plume from the mock-up. The significant temperature interruptions could have been due to loose thermocouple connections. In regard to spraying with faster robot speed (figure 5), more passes of the spraying system were needed to achieve the required layer thickness, which is reflected by the higher number of temperature changes than during normal spraying speed. Furthermore, special attention was paid to achieving a lower maximum temperature than with normal speed, which was realized by removing the plasma plume more often from the mock-up. Consequently, maximum temperatures about 100 °C lower than with normal speed were accomplished at the same distances from the substrate top-surface. Hence, the faster spraying speed improves the coating in two ways: first, the local temperature increase is not as fast and secondly, due to the lower amount of deposited material per pass, it could be possible to produce a coating with a more even structure.

After coating, no apparent external defects—e.g. delamination or cracks—were observed. To remove the unattached powder from the mock-up, cleaning with an ultrasonic bath and dry ice blasting were tested, of which the latter produced better results and can also easily be used for larger components. A subsequent, corroborative defect control by dye penetration was also tried out, but produced no usable results, due to the surface roughness of the coating ($R_a \approx 6.5\ \mu$m [3]) and porosity (<5% [3, 5]).
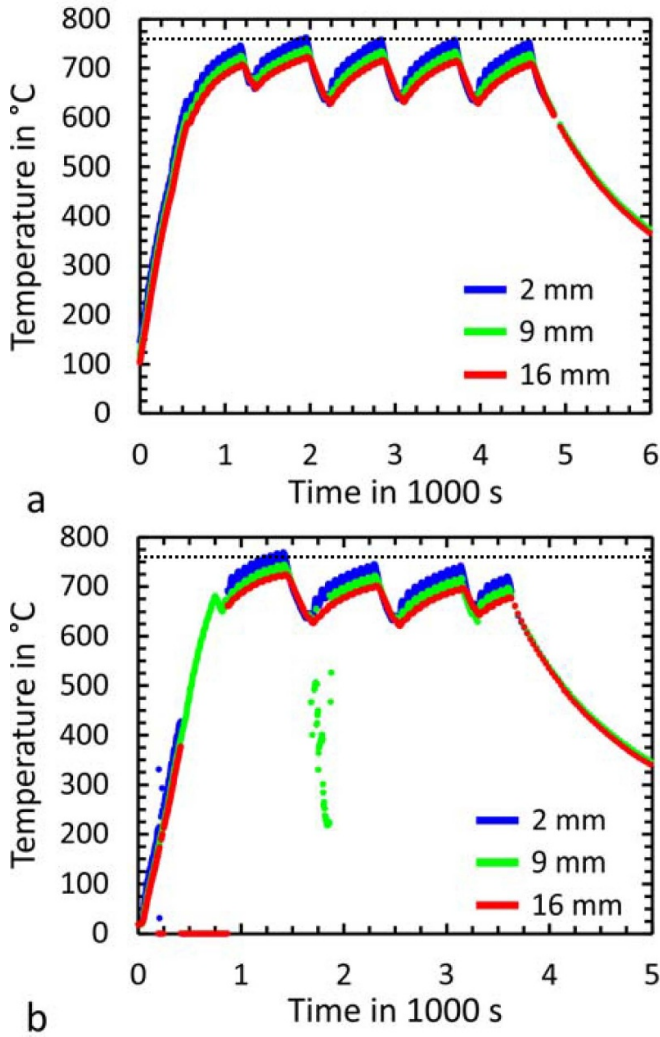
without powder injection. The surface and internal temperature of the mock-ups during spraying were monitored using a pyrometer and by three implemented type-K thermocouples, respectively.

Figure 4. Temperatures in the first mock-up, at different distances from the substrate top-surface, during coating (*a*) the FG-layer and (*b*) the W-top coat at normal spraying speed. The dotted horizontal line marks the nominal temperature limit given by EUROFER's annealing temperature of 760 °C.
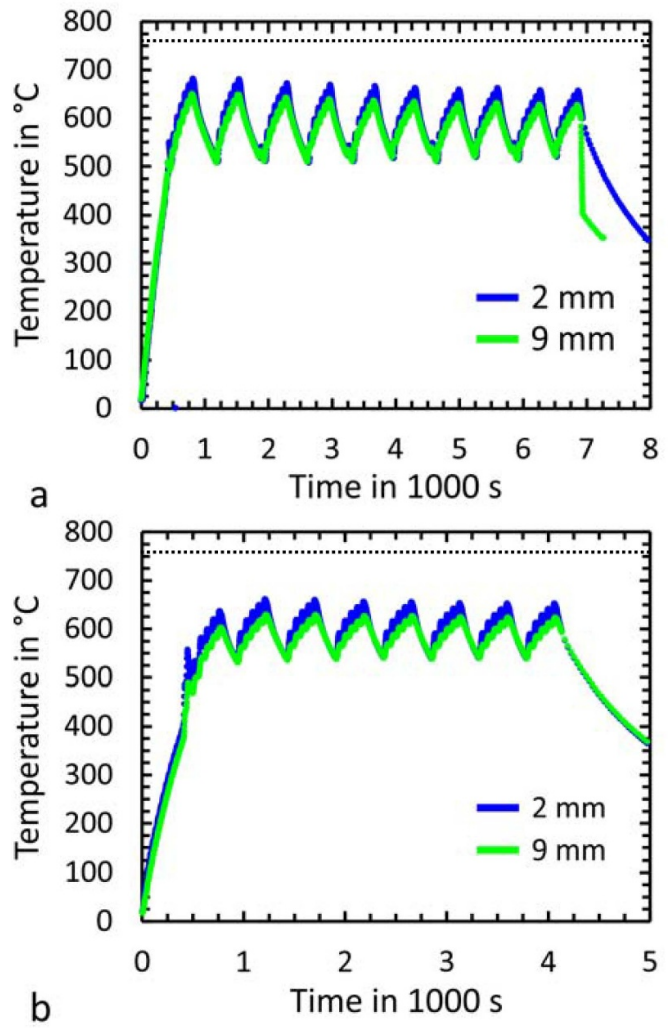

Figure 5. Temperatures in the second mock-up, at different distances from the substrate top-surface, during coating (*a*) the FG-layer and (*b*) the W-top coat at faster robot spraying speed. The dotted horizontal line marks the nominal temperature limit given by EUROFER's annealing temperature of 760 °C.

The coatings were also controlled for internal defects by ultrasonic testing at a frequency of 10 MHz using longitudinal sound waves. For the coating an average sound velocity (5416 m s^{-1}) was estimated, based on the sound velocities of W (5200 m s^{-1}) and steel (5560 m s^{-1}), the corresponding FG-layer compositions and nominal thicknesses. Based on this average sound velocity and the measured signal travel time, the distance of the echo source is determined. This allows to analyze the produced information at a specific depth, which is exemplarily shown in figure 6 for the mock-up coated with normal spraying speed. Depicted are the coating after dry ice blasting and the results of the ultrasonic testing for the calculated depth of 2–4 mm and 6–8 mm. These results are a 2D presentation of all discontinuity echoes within these two depth regions representing the coating/substrate interface and the cooling channels, respectively. In regard to the interface, the results indicate that the signal amplitude is evenly reduced over the whole coating area, while in the latter all cooling channels are clearly depicted. Hence, no significant internal

defects, like internal delamination, exist. In the case of the mock-up coated applying faster robot speed, similar results are observed.

Due to the encouraging results it was decided to test one mock-up under fusion relevant conditions. For the test, the mock-up coated with normal spraying speed was selected, because of the higher substrate temperatures during coating, which could have led to better coating adhesion, thus lowering the risk of layer spall-off during the experiment. To ensure a homogeneous He distribution in all cooling channels, new manifolds were developed to replace the simple ones (figure 7). The manifolds were fabricated out of the FM-steel 1.4901, due to the availability of suitable thick plates, and attached to the plate of the mock-up by TIG-welding. Afterwards the mock-up was subjected to post welding heat treatment (PWHT) in a vacuum furnace for 2 h, however, at a lower temperature of 740 °C than for the previous manifolds, followed by furnace cooling. The vacuum furnace was used to avoid oxidation of the W-coating, while 740 °C is the low-
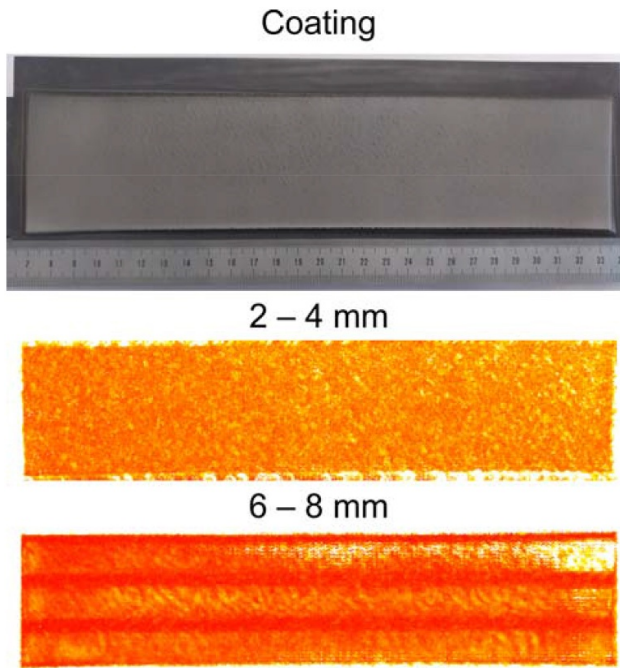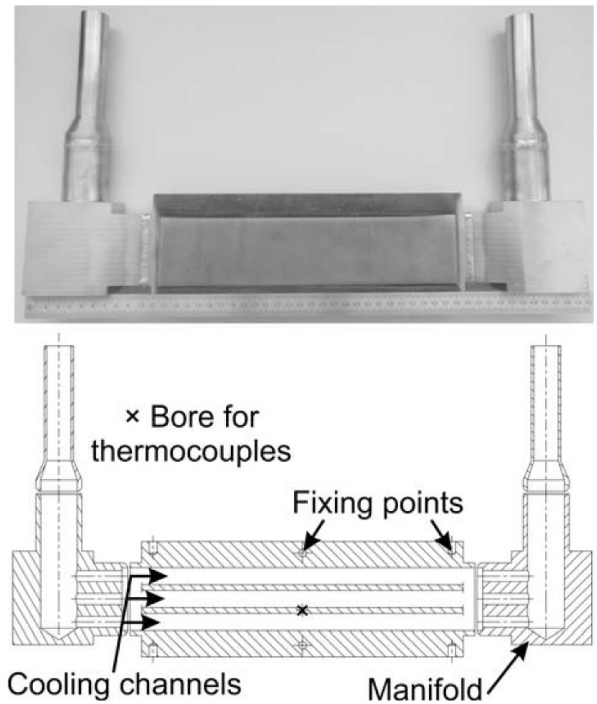
Figure 6. A top view of the first mock-up, coated at normal spraying speed, after dry ice blasting, and the results from ultrasonic testing below as a 2D presentation of all discontinuity echoes within the two specified depth regions representing the coating/substrate interface and the cooling channels, respectively.

Figure 7. Top view and schematic cross-section of the mock-up, coated with normal spraying speed, after welding the new manifolds.

est allowable annealing temperature, according to [13], and was chosen to prevent formation of Fe/W IMC [9]. After PWHT, the coating still adhered to the plate and exhibited no defects. However, radiographic inspection of the welding seams indicated the presence of defects that required repairing. As a consequence, the manifolds were re-welded and the mock-up was again subjected to PWHT.

This latter procedure caused the warping of the substrate plate in the range of about 1 mm transversal to the longitudinal axis of the mock-ups and spall-off from the W-top coat, whereas the FG-coating still adhered to the substrate and showed neither external nor internal signs of delamination, as indicated by ultrasonic testing. Furthermore, the W-fracture exhibits surface plastic deformations and powder splat pull-offs at several locations (figure 8), indicating that relevant adhesion exists between the FG-layer and the W-top-coat. Hence, the warping of the substrate, and perhaps also the many processing steps, produced a residual stress and strain state in the whole mock-up, which exceeded the layer adhesion strength and finally caused the W-top-coat to spall off. Parts of this spalled-off W-coating were used for measuring the thermal diffusivity of the W-top coat. As the still-adherent FG-coating showed no signs of delamination, the mock-up was subjected to a pressure test, according to the provisions of the European design code for pressure vessels DIN EN 13 445.

3.2. Testing conditions and thermal fatigue tests of FW mock-up

3.2.1. Determination of test conditions.
The aim of testing the FW mock-up in HELOKA was to confirm the durability
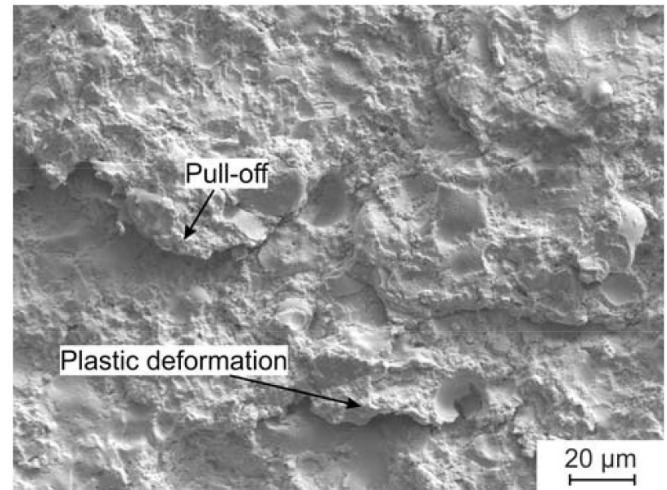
Figure 8. Fracture surface of the spalled-off W-top coat.

of the coated mock-up by exposing it to fusion-relevant heat loading in the form of thermal cycles. This type of loading was first of all selected to generate similar conditions in the mock-up like in future breeding blankets during normal operation. Secondly, cyclic thermal loading will put the mock-up under higher strain, i.e. thermal fatigue, than holding it at a constant high temperature. The difference should be particularly pronounced for this system, because with higher temperatures the system approaches its coating temperature and thus the residual stresses developed during cooling from the coating
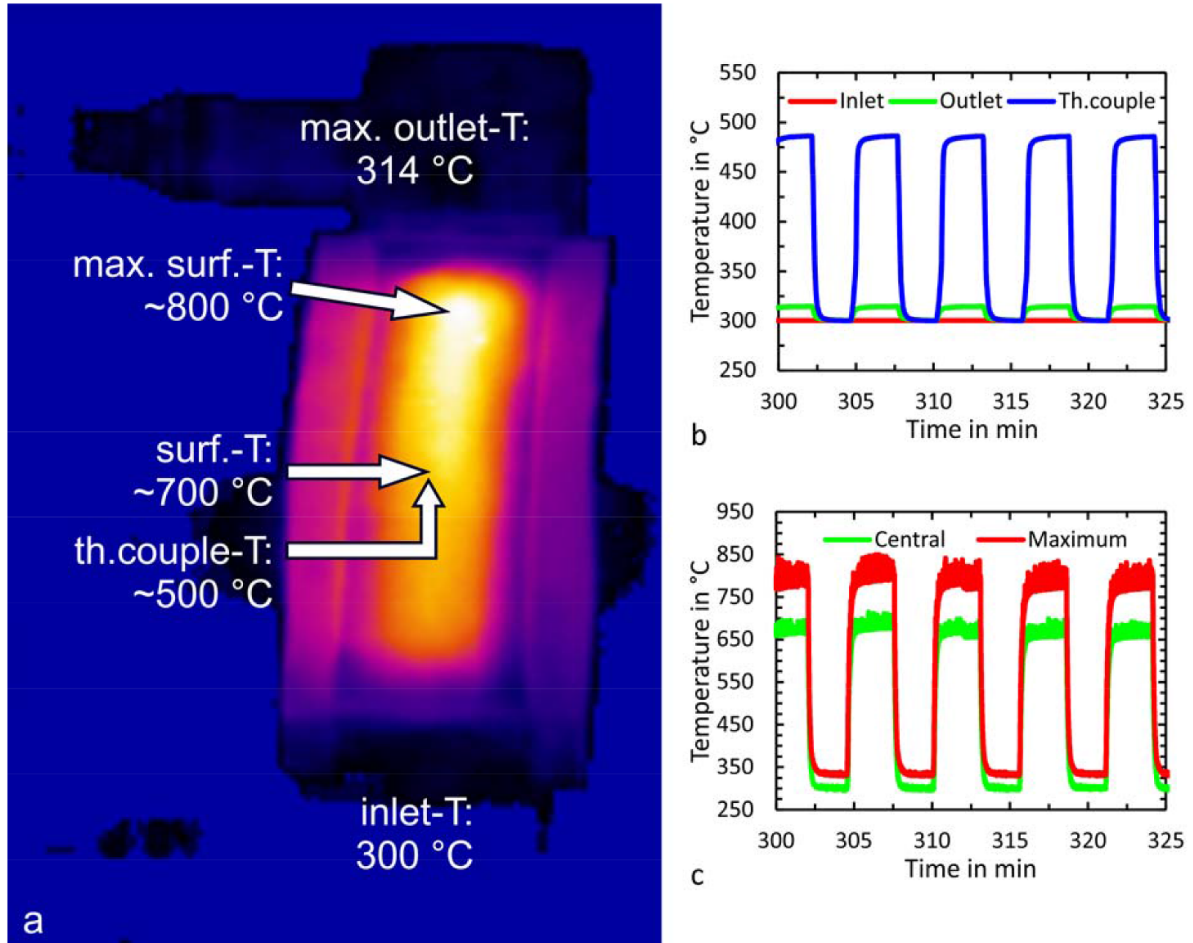
Figure 9. Recordings of the mock-up during testing in HELOKA with (*a*) a thermal image at maximum heat load, (*b*) internal and (*c*) external temperatures.

Table 3. Applied parameters for the thermo-hydraulic extrapolations.

Parameter	Value
Temperature	320 °C
Pressure	8 MPa (abs.)
Dynamic viscosity, μ	3.206×10^{-5} Pa s
Heat conductivity, λ_{He}	0.257 W (m K)$^{-1}$
Canal cross-section, A	1.466×10^{-4} m^2
Characteristic length, d_h	1.259×10^{-2} m

temperature diminish due to the thermal mismatch between the substrate and coating.

The required test parameters were determined by a simplified procedure in the form of one dimensional calculations, as presented in [14]. For the calculation, a single channel with the length L and the width w is considered. Furthermore, it is assumed that this channel receives only one uniform heat flux from one side with the density $\dot{q}$, while He flows with a mass flow rate of $\dot{m}$, an inlet temperature of T_1, and a mean specific heat capacity $\overline{c_p}$ through the channel. The resulting He outlet temperature T_2 can be computed by the equation [14]:

$$T_2 = T_1 + \frac{\dot{q} L w}{\dot{m} \, \overline{c_p}}. \tag{1}$$

In regard to the produced mock-ups, the channel dimensions L and w are 0.3 and 1.5×10^{-3} m, respectively, with a filet radius of 2×10^{-3} m. In the case of He, a mass flow in the range of $0.04 \leq \dot{m} \leq 0.07$ kg s^{-1}, with an inlet temperature of 300 °C and pressure of 8 MPa is chosen. The mean specific heat capacity equals 5193 J (kg K)$^{-1}$ [15], under the assumption of isobaric behavior. Finally, a heat flux density in the range of $0.5 \leq \dot{q} < 1$ MW m^{-2} [14] is expected. Hence, the outlet temperature will be in the span of about 306 °C to 322 °C.

To identify the maximum surface temperature T_{max} of the FW, the calculated He outlet temperature can be implemented into equation [14]

$$T_{max} = T_2 + \dot{q} \left(\frac{1}{h} + \frac{s}{\lambda} \right) \tag{2}$$

as it is of interest not to exceed the maximum working temperature of the materials. The wall material is represented by its thickness s, between the heated and the cooled surfaces, and its heat conductivity λ. For the mock-ups the wall thickness equals 4×10^{-3} m, while λ is calculated, for an average temperature of 400 °C, as 30.12 W (m K)$^{-1}$ by equation (9) from [12].

7

Table 4. Maximum surface temperatures depending on heat flux density and He mass flow.

$\dot{m}$ in kg s^{-1}	$\dot{q}$ in MW m^{-2}:	0.50	0.55	0.60	0.65	0.70	0.75
	h (+10%) in W m^{-2} K^{-1}			T_{max} in $^{\circ}$C			
0.04	3542	518.4	540.2	562.1	583.9	605.7	627.6
0.05	4043	498.7	518.6	538.5	558.3	578.2	598.1
0.06	4505	484.6	503.1	521.5	540.0	558.5	576.9
0.07	4936	473.9	491.3	508.7	526.1	543.4	560.8

Table 5. Comparison of the test criteria and parameters applied to the mock-up in HELOKA.

Parameter	Criteria	Applied
Pre-heating temperature	300 $^{\circ}$C	300 $^{\circ}$C
Helium inlet temperature	300 $^{\circ}$C	300 $^{\circ}$C
Helium pressure	8 MPa (abs.)	8 MPa (abs.)
Helium mass flow per channel	70 g s^{-1}	56.67 g s^{-1} (averaged)
Heat flux density	$\rightarrow$0.7 MW m^{-2}	0.7 MW m^{-2} (average)
Heating/dwell time	–	180 s/150 s
Substrate temperature	$\leq$550 $^{\circ}$C	$\leq$520 $^{\circ}$C
Surface temperature	$\leq$800 $^{\circ}$C	$\leq$800 $^{\circ}$C
Number of cycles	1000	1000

The heat transfer coefficient h from the solid wall into the He stream, on the other hand, has to be determined specifically for this channel geometry and He mass flow. The calculation is performed according to the thermo-hydraulic extrapolations presented in [14], namely table 3 and equation 8, which allow easy and fast determination of a good approximation for the heat transfer coefficient for a smooth duct:

$$h = 0.164 \left(\frac{d_{h} \frac{\dot{m}}{A}}{\mu} \right)^{0.593} \left(\frac{\lambda_{He}}{d_{h}} \right) \quad (3)$$

The required He properties are determined for the outlet side, because that is where the highest temperatures are to be expected, for a temperature of 320 $^{\circ}$C by using the VDI heat atlas [15], and are listed in table 3.

Because this extrapolation is considered conservative in the literature [14], as the estimated heat transfer values lie about 10%–15% below the experimental values, the heat transfer coefficient calculated by equation (3) is increased by 10% for the computation of the maximum surface temperatures. The T_{max} acquired in this way for a range of heat flux density and He mass flows are listed in table 4.
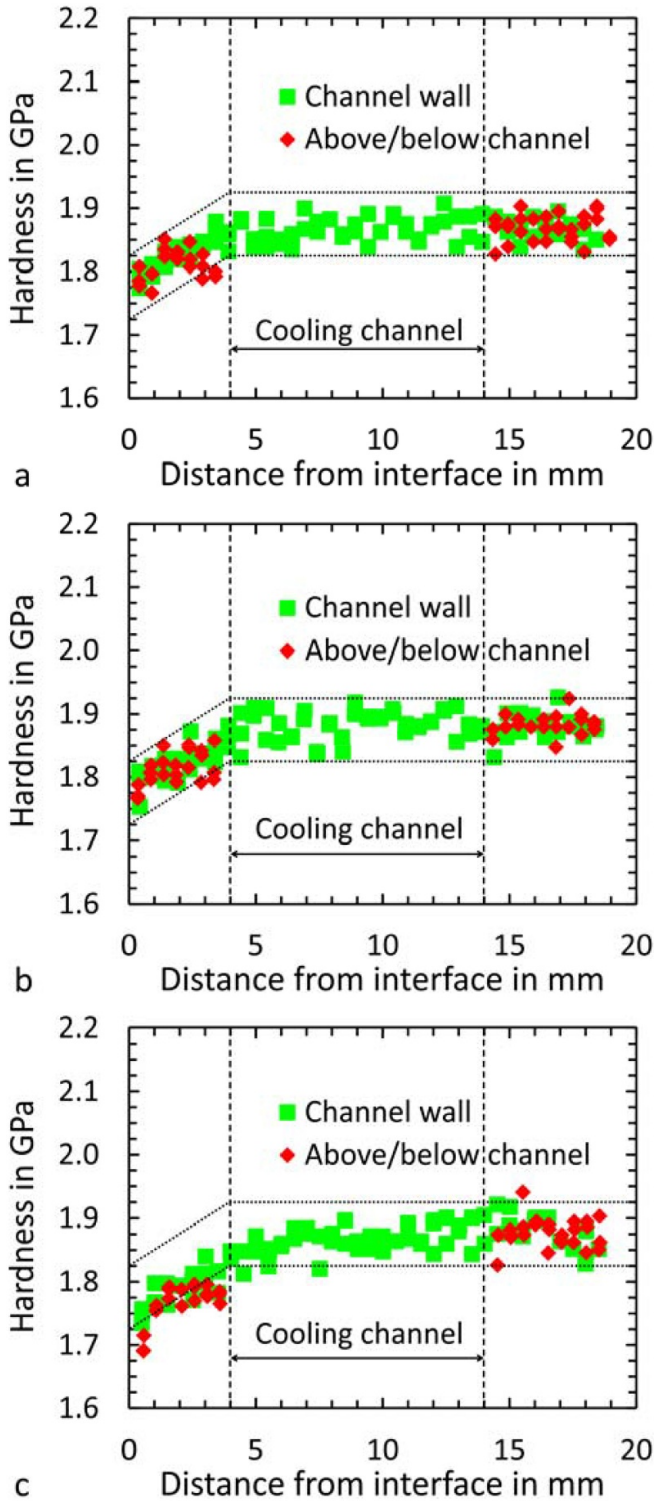
First of all, all the parameter combinations that cause temperatures above the maximum EUROFER temperature of 550 $^{\circ}$C can be derived from this matrix and excluded in advance. The light gray highlighted fields indicate with which parameter sets temperatures close to 550 $^{\circ}$C can be achieved and thus the highest heat loads that can be applied. Hence, for a preferably high heat load towards 0.7 MW m^{-2} an average He usage of up to 70 g s^{-1} is required. In addition to this estimation, the substrate and coating surface temperatures were monitored during the tests, first of all to evaluate the resulting temperatures, and secondly, to assure that the respective maximum temperatures of 550 $^{\circ}$C and 800 $^{\circ}$C were not exceeded to avoid the formation of Fe/W IMC [9]. Finally, the mock-up was homogeneously pre-heated by He to 300 $^{\circ}$C, to reach breeding blanket operation temperatures and to avoid additional thermal stresses, as indicated in [7]. To prevent the build-up of constrain stresses as well the mock-up was mounted constrain free in the facility.

3.2.2. Procedure of thermal fatigue tests. For monitoring the mock-up coating surface temperature and internal temperature, a thermo-camera (figures 9(*a*) and (*c*)) and a thermocouple (type-K) (figure 9(*b*)) were used, respectively. The latter was implemented into the hole in the center of the plate and the temperature measured 2 mm below the substrate/coating interface. The substrate temperature was further decreased to 520 $^{\circ}$C for the experiments, to minimize the risk of a mock-up failure inside the test facility, in addition to the pressure vessel safety control. Considering also that a thermal gradient forms along the mock-up, the maximum temperature at the thermocouple was set to 500 $^{\circ}$C, so that on the plate outlet side 520 $^{\circ}$C is not exceeded. In parallel to the use of the thermo-camera and thermocouple, the inlet and outlet He-temperatures (figure 9(*b*)) were measured by the HELOKA facility and in this way the received surface heat flux was calorimetrically evaluated.

In view of the thermal loads, pre-heating was achieved by slowly increasing the He-temperature in the loop, e.g. when starting at room temperature over the course of about 3 h. Regarding the heat flux density and pulse lengths, an additional preliminary procedure was conducted. In the case of the heat flux density, its power level was increased in three steps: first the power level was low to fix the scanning pattern of the facility electron beam on the coated area of the mock-up, then the level was set to about 0.5 MW m^{-2} to determine the pulse length that would allow the calorimetric evaluation of the surface heat flux, and finally, the level was set close to the chosen value, while monitoring the maximum temperatures. In contrast to the estimation, however, a comparatively lower He mass flow was sufficient to keep the temperatures below their respective limits. In the case of the pulse lengths, a heating duration of 180 s was selected, to have a

Figure 10. FW plate hardness profiles, with additional boundary lines as orientation guides, of the mock-up tested in HELOKA at (*a*) the inlet, (*b*) the outlet side and (*c*) from the high-temperature area during exposure (figure 9).
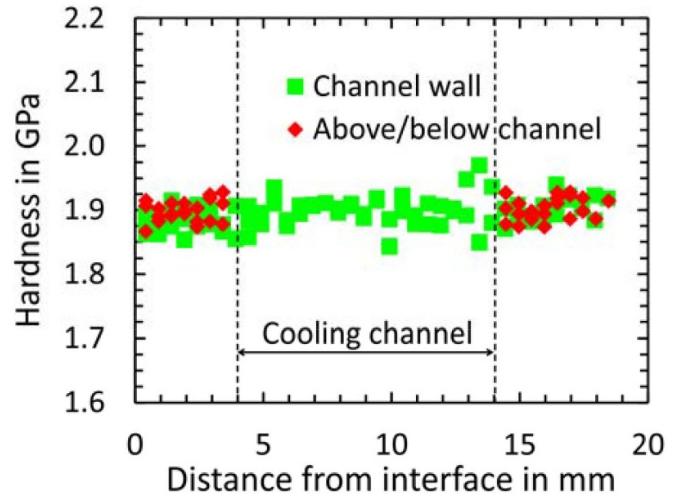
Figure 11. FW plate hardness profiles of the mock-up coated at a lower maximum temperature.
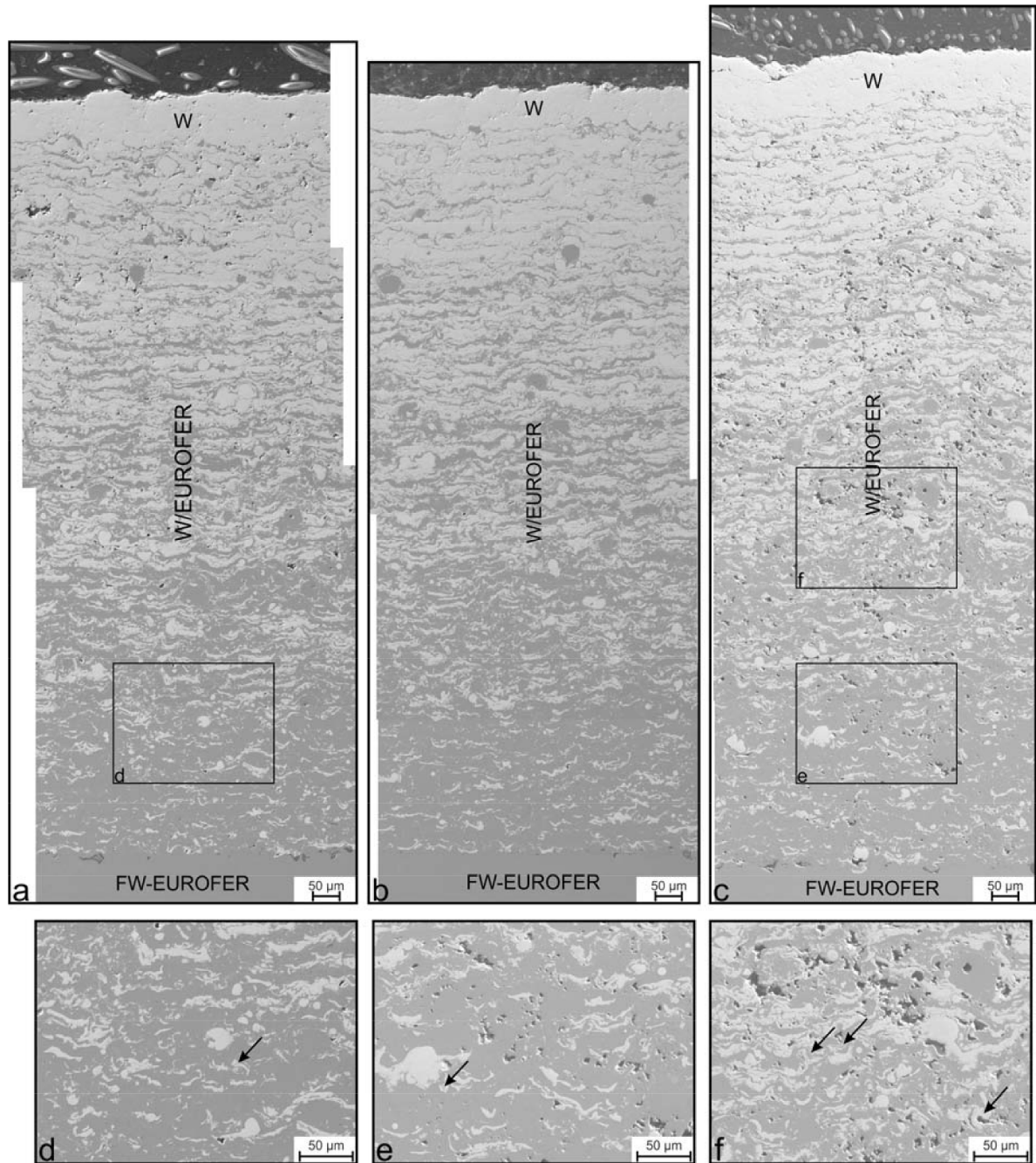
Consequently, the pulse length is mainly determined by the measurement of the He-outlet temperature and thus also by the thermal capacity of the respective manifold. An overview of the test criteria and final test parameters is given in table 5.

3.3. Post exposure analysis

During thermal cycling no hotspots formed, which indicates that the coating did not detach during the heat flux tests. After the exposure, material samples were cut out of the mock-up by EDM. On these samples, microstructural analyses were carried out to investigate whether the substrate-layer system changed or the coating interfaces may have deteriorated. The possible change of the substrate because of local excessive temperatures was evaluated in the form of hardness profiles, which were determined by using a Vickers indenter with a load of 9.81 N (HV1) and a minimum indent distance of 0.5 mm. As reference, the hardness profile at the inlet is considered where the temperatures are too low to cause any change.

In this way, qualitatively identical FW hardness profile trends (figure 10) were determined at the inlet and outlet side of the mock-up and a similar trend from the area below the maximum surface temperature during testing (figure 9(*a*)). Compared to the hardness profiles of the second mock-up (figure 11), which was specifically coated at a maximum temperature about 100 °C lower, the substrate tempering temperature of the first mock-ups was thus apparently slightly exceeded during the coating process, as hardness loss exists but is limited to a depth of about 4 mm. It also follows from these hardness profiles that the heat did not accumulate locally above the channels, possibly due to the smaller amount of material, which would have led to different temperatures and thus hardness losses.

In view of the quantitative hardness values at the three different locations, the sample from the high-temperature area (figure 10(*c*)) exhibits, despite the scatter, a nearly 2 mm deeper and more distinct hardness loss, about 0.05 GPa,

stable He-temperature reading at the outlet of the mock-up and thus a reliable evaluation of the surface heat flux. The dwell time (150 s), on the other hand, followed from the observations of the preliminary tests and is the shortest duration after which the He-temperature at the outlet returned to 300 °C.

Figure 12. Cross-sections after thermal testing in HELOKA from (*a*) the inlet side, (*b*) the outlet side, (*c*) the high-temperature area (figure 9) of the mock-up, and (*d*) to (*f*) the higher magnification of the marked areas.

than the other two samples (figures 10(*a*) and (*b*)). As additional hardness loss caused by temperatures above the tempering temperature can be ruled out, this indicates that in this area the number of thermal cycles, and particularly the temperatures, were sufficient to allow significant thermo-cyclic softening.

In regard to the microstructure of the coatings, the first aspect that catches the eye in the sample cross-sections (figure 12) is that apparently not all the W-top coat has spalled off, but about 50 to 100 μm still adheres to the FG-layer. Additionally, the cross-sections reveal that the

FG-layer is about 100 to 200 μm thicker than specified, while the coating microstructures are generally similar to each other. At all three locations the coatings exhibit no deterioration of the coating/substrate interface, in the form of delamination or crack growth parallel to the coating/substrate interface. Hence, the thermal conductivity of the whole coating system did not diminish, which corroborates the observations made with the thermo-camera during testing.

On the other hand, figure 12(*c*) depicts areas with a comparably higher amount of pores or cavities that appear locally
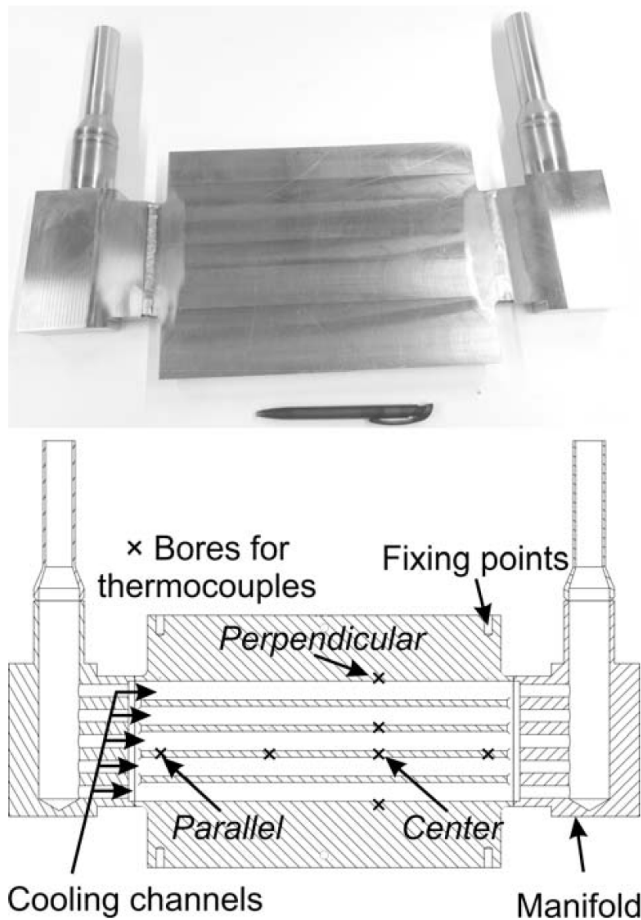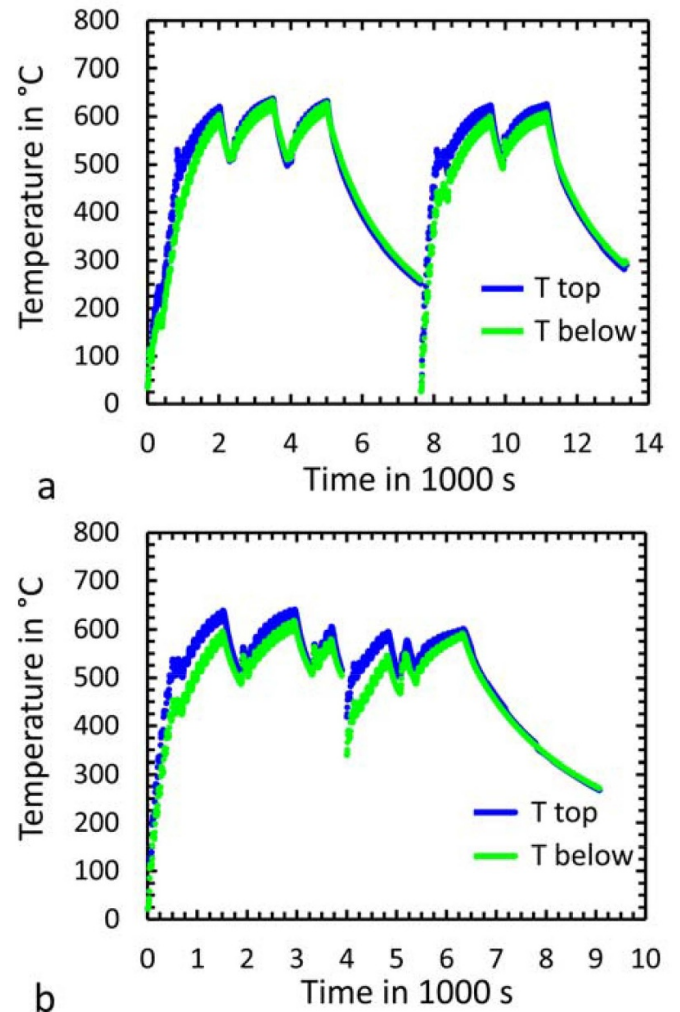
Figure 13. The second kind of mock-up after fabrication and its schematic cross-section, with three particular thermocouple positions used for temperature monitoring.

Figure 14. Temperatures in the larger mock-up, at different distances from the substrate top-surface, during coating (*a*) the FG-layer and (*b*) the W-top coat.

in the sample. As a possible origin the production process can be ruled out first, because of the irregular local appearance of the cavities. Also the growth or coarsening of pores seems unlikely, since the other two regions exhibit no significant amount of small pores. It could be, however, that some coating particles broke out of the cross-section during preparation, due to the loss of adhesion between the particles and their volume remains as these cavities. The possibility of particle loss is further emphasized by the figures made at higher magnification (figures 12(*e*) and (*f*)) from the high-temperature area, which show that the cavities have comparable size and shape like the brighter appearing W-particles. The de-bonding of the particles could have been induced by the mismatch in CTE on the microscopic scale between the individual W/steel particles under thermal cyclic loading. The extent to which such de-bonding was also influenced by residual stresses cannot be determined, due to the welding and PWHT- induced warping as well as spall-off from the W-top coat.

Furthermore, at high magnification some particles and areas, having a gray scale between those of W- and steel-particles, can occasionally be found in all three cross-sections, as exemplarily indicated by the arrows in figures 12(*d*)–(*f*). Based on the results of EDX spot analyses, these particles

could be types of (Cr-)/Fe/W IMC [16]. Since these particles appear neither in the high-temperature areas towards the coating surface and only in the FG-layer at or below the W/steel ratio of 50/50, nor equally at the interfaces of the particles, it is very likely that they did not precipitate during testing. Hence, these particles originated from the production process and could be, due to the large coated and analyzed area, a statistical appearance. In particular, the large coating area increases the possibility for IMC, due to the higher amount of sprayed powder and thus the chance for in-flight particle reactions. Reactions inside the deposited coating are for these mock-ups, on the other hand, unlikely, as the substrate temperatures were monitored and stayed clearly below 800 °C during the coating process.

Therefore, these observations underline the thermal stability of the coating, especially as this area experienced thermal loads for a much longer time—at least 2000 min based on the duration at maximum temperature (figure 9(*c*)) times the number of cycles—than the material samples reported in [9] (60 min). Secondly, the investigations revealed no apparent
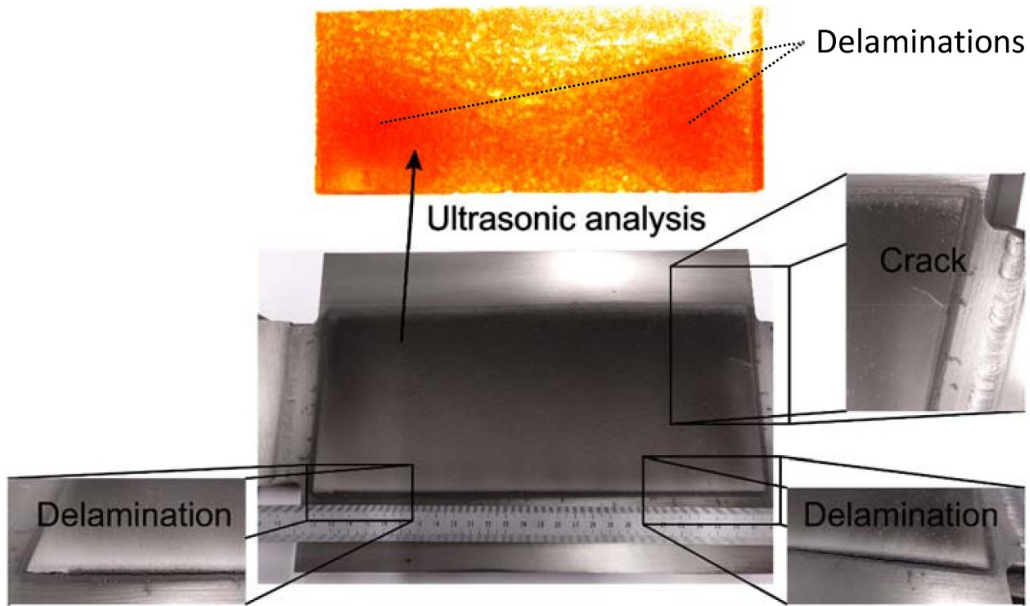
Figure 15. Top view of the larger mock-up, after the first coating and ultrasonic testing results.
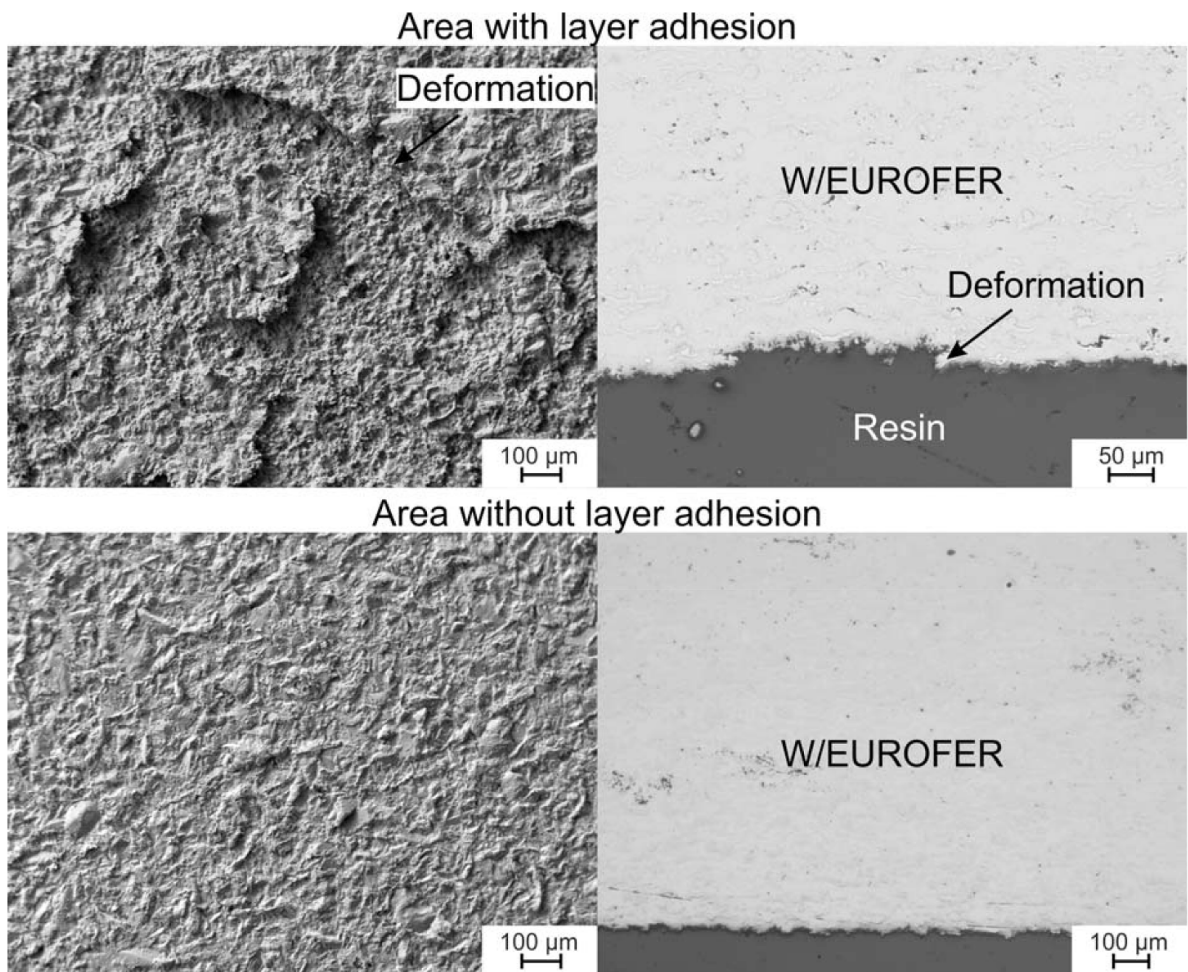

Figure 16. Surfaces and cross-sections of the removed coating at the coating/substrate interface in an area with and without layer adhesion.
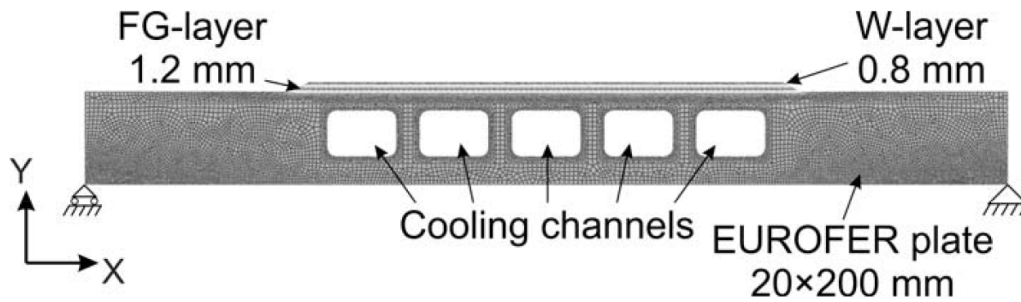
Figure 17. Model of the mock-up cross-section with a mesh for the thermomechanical simulations.
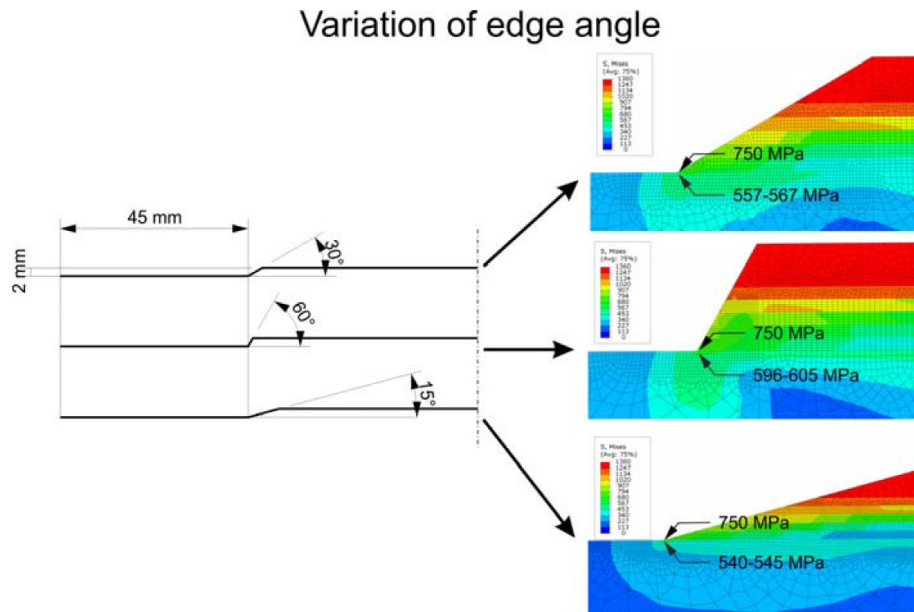

Figure 18. Von Mises stresses at the coating edges as a function of the edge slope.

detrimental effect of the IMC on the coating, which could have been due to the low amount and their small size.

To conclude, the test emphasizes the durability of the coating system under fusion-relevant conditions. For future tests, it is of high interest to explore how the layer system performs for significantly longer test durations or higher numbers of thermal cycles. During such tests the thermo-mechanical behavior—in particular thermo-cyclic softening or the release of residual stresses—of the coating system with a complete 0.8 mm thick W-top coat and without any additional influence from welding, needs to be investigated.

4. Production and coating larger FW mock-ups

4.1. Coating using previous production process

Encouraged by the successful coating of the mock-ups another larger mock-up was produced, parallel to the pressure vessel qualification and heat flux tests in HELOKA of the smaller mock-up, in view of coating a future full scale FW. The mock-up was manufactured out of an available $300 \times 200 \times 20$ mm^3 large EUROFER plate with five cooling channels that have rectangular cross-sections of 10×15 mm^2

with a 2 mm filet radius (figure 13), wall thicknesses to the top surface and in between the channels of 4 mm and 5 mm, respectively, as well as special V-shaped ribs on the top side that increase the heat transfer between the plate and the cooling medium [14, 17]. At seven different locations, lengthwise and crosswise to the longitudinal axis of the plate, Ø 1.5–18 mm holes were drilled into the cooling channel walls to insert thermocouples. In particular, three positions relative to the longitudinal axis of the cooling channels were used for monitoring the temperatures during the coating process. For this mock-up the further developed manifolds, made out of 1.4901 and with internal 90° turns, were used and attached to the plate by TIG-welding. Afterwards, a complete hardening and tempering heat treatment was performed, similar to the previous kinds of mock-up.

For coating, the plate was preheated by the plasma plume without powder injection, while the coating itself was also applied to the central part above the cooling channels covering an area of 270×115 mm^2. The coating was defined to consist of a 1.2 mm thick FG-layer with a 0.8 mm thick W-top coat and was applied to the mock-up with a spraying system speed of 0.5 m s^{-1}. A cover plate protected the holder, the side parts and especially the welding seams as well as the connecting

Table 6. Implemented elastic [8] and plastic [6] material properties for EUROFER and W.

|	EUROFER					Tungsten		
Temperature in °C	Young's modulus in MPa	Yield strength in MPa	Ultimate tensile strength in MPa	Failure strain	Coefficient of thermal expansion in K^{-1}	Young's modulus in MPa	Yield strength in MPa	Coefficient of thermal expansion in K^{-1}
20	217 260	545.57	794.61	0.1677		397 938	1360.46	
200	207 327	483.62	620.71			397 270	1154.17	
300				0.1309				
400	197 123	446.99	576.74	0.1362	1.20E-05	394 480	947.86	4.40E-06
500				0.1775				
600	177 589	298.32	509.05	0.2659		389 508	764.79	
700	161 024	134.79	380.32	0.2963		386 210	681.67	
900	55 800	50	220.67			377 970	531.74	
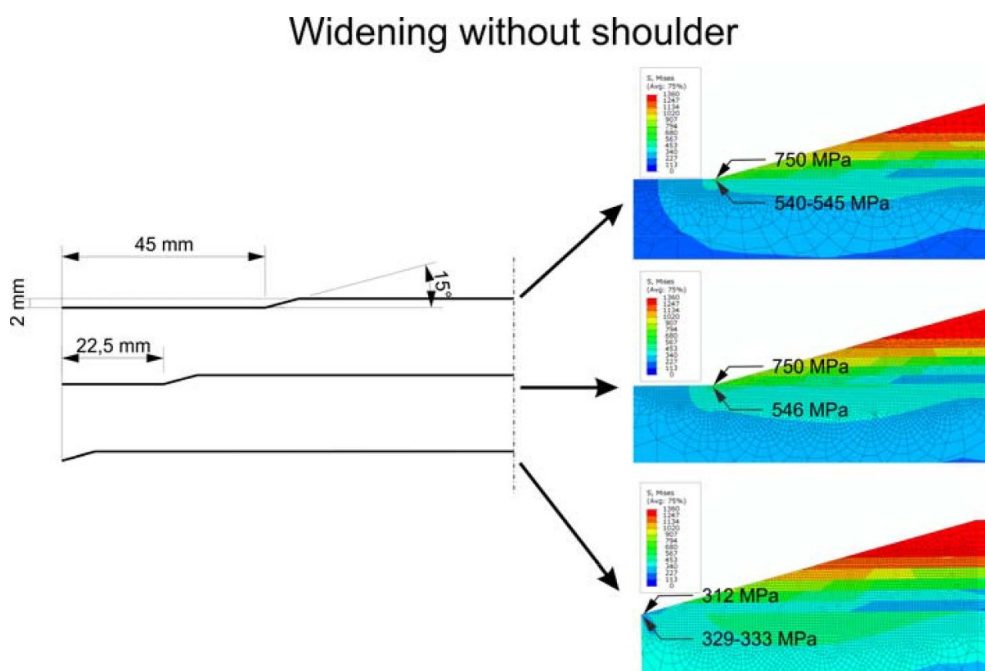
Figure 19. Von Mises stresses at the coating edges as a function of the whole coating width.

Table 7. Applied EUROFER properties for the heat transfer simulations [12].

| Temperature in °C	Thermal conductivity in W $(mm\ K)^{-1}$ (equation 9)	Specific heat in J $(g\ K)^{-1}$ (equation 6)	Density in g mm^{-3}
20	0.029333471	0.44810195	
200	0.031102651	0.51847092	
400	0.030119782	0.58454167	
600	0.031595950	0.79260167	0.00775
700	0.034995500	0.99990265	
800	0.042829894	1.30273094	
900	0.064402723	1.72109655	

tubes. Figure 14 depicts the internal temperature trends in the central area during deposition of the FG- and the W-layer. Like for the second test mock-up, maximum temperatures about 100 °C lower than the tempering temperature were achieved. The interruptions and restarts were due to problems with the facility: firstly as the heat management capacity of the facility

was reached due to the large substrate, and secondly as some layer material spalled off from the cover plate and blocked the manipulator mechanisms.

After coating, a crack and delamination were observed externally at the corners of the coating (figure 15). In view of the ultrasonic analysis, the signal amplitude is significantly
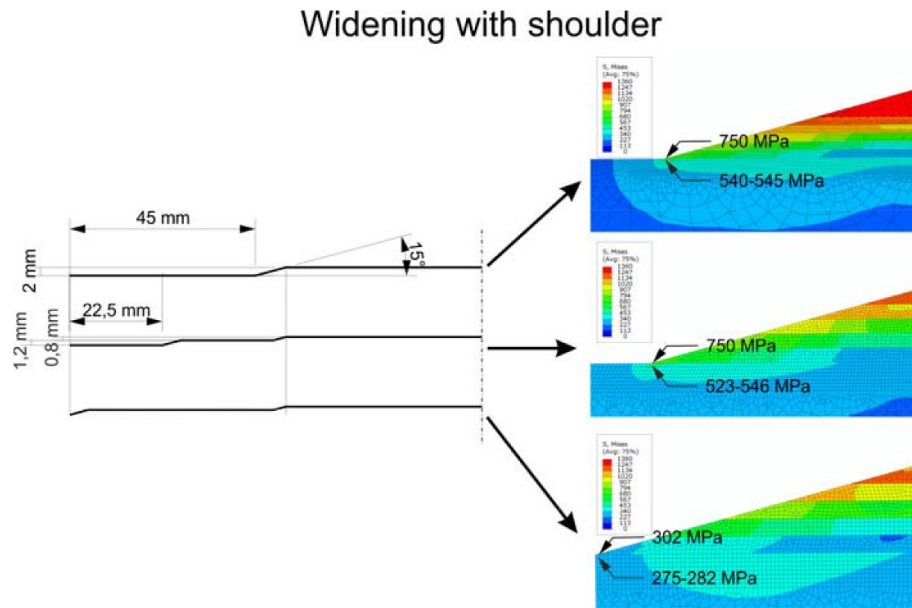
Figure 20. Von Mises stresses at the coating edges as a function of the FG-coating width.
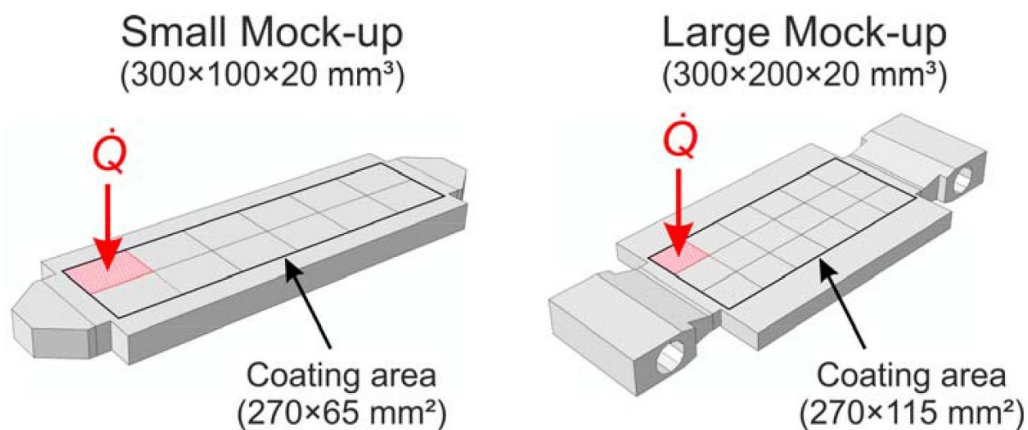
Figure 21. Models used for the simulations of the temperature distributions.

reduced near the externally visible delaminations. This implies that the delamination extends further beneath the surface, so that only about one third of the area of the coating adheres to the substrate.

For a new deposition, the layer system was removed and the substrate surface was refurbished by mechanical means. Parts of the removed coating were used to measure the thermal diffusivity of the whole layer system, shown above. In regard to its microstructure, the removed coating exhibits an uneven fracture surface in the area with adhesion (figure 16) with plastic deformation, indicating that the structure adhered to the substrate and failed inside the coating itself during removal. In the case of the coating in the area without adhesion, however, a comparatively even surface is visible, implying that the coating was already detached from the substrate before removal. Hence, either the produced adhesion was too weak to compensate for the layer residual stresses or sufficient bonding between the substrate and the first coating layer was not even produced.

To realize, notwithstanding, a successful coating two aspects were considered for modification: first, the layer cross-section could be modified to reduce the local maximum mechanical stresses; secondly, the coating process could be adjusted to adapt to the larger component size, i.e. the preheating is adjusted to heat the higher thermal mass of the mock-up to a required temperature level for the formation of metallurgical bonding. The effects of these modifications were evaluated by FE-simulations, using the software ABAQUS [18], and in this way the spraying process was optimized for the new coating.

4.2. FE-optimization study for coating larger areas

4.2.1. Coating design. The modifications of the coating design were analyzed on a cross-section of the mock-up by thermomechanical simulations (figure 17). The designs were evaluated to minimize the von Mises stresses at the FG-layer edges.

For EUROFER and W, the thermomechanical properties used are listed in table 6. They are particularly those of
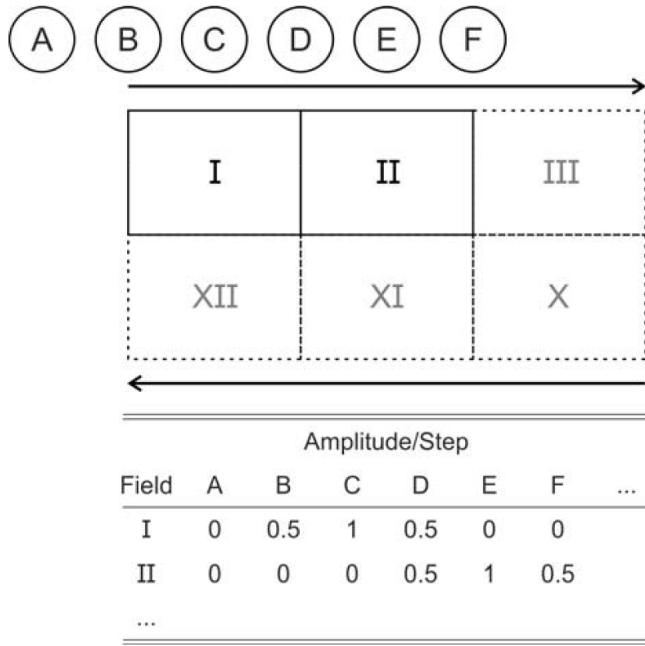
Figure 22. Heat flux amplitudes on the individual fields of the coating area as a function of time.

bulk materials as the properties of VPS materials, especially those sensitive to microstructure, are not yet available. In regard to the FG-layer, the area was divided into five 240 μm thick sections and the material properties linearly interpolated to the corresponding W/EUROFER ratio. For W and the FG-layer, linear-elastic and ideal-plastic material behavior was assumed. In the case of EUROFER, linear-elastic behavior was also assumed and for plastic deformation additionally isotropic hardening, based on its ultimate tensile properties, was considered. The mesh consisted of 'generalized plane strain' elements with a primarily quadratic form. Their maximum edge length was in the range between 0.06 and 1 mm, with the smaller value especially being used for the coating and the local area beneath the coating edges.

The simulation was conducted in the form of a static analysis, by cooling down the homogeneous temperature field of the cross-section from its stress free state at 750 °C to 20 °C. The lower right corner of the EUROFER plate was fixed in the *x*- and *y*-direction, while the lower left corner was restricted only in the *y*-direction.

In terms of the coating edge slopes, at a constant width of uncoated area, an increase of the angle (e.g. 60°) leads to higher stresses at the corner of the coating particularly in the substrate (figure 18). For smaller angles (e.g. 15°), on the other hand, the stress fields are more evenly distributed, while beneath the edge the stress values are lower. Therefore, edge slopes lower than 30° are foreseen for the new coatings.

In view of the coating area (figure 19), an increase onto 50% of the previously uncoated side areas leads to similar von Mises stress values beneath the edge, whereas fields with von Mises stresses of about 340 to 570 MPa are broader. In case the coating is deposited on the whole width of the mock-up, the stresses at the coating edge tip in the substrate and in the coating itself are significantly lower, which may be due to lower
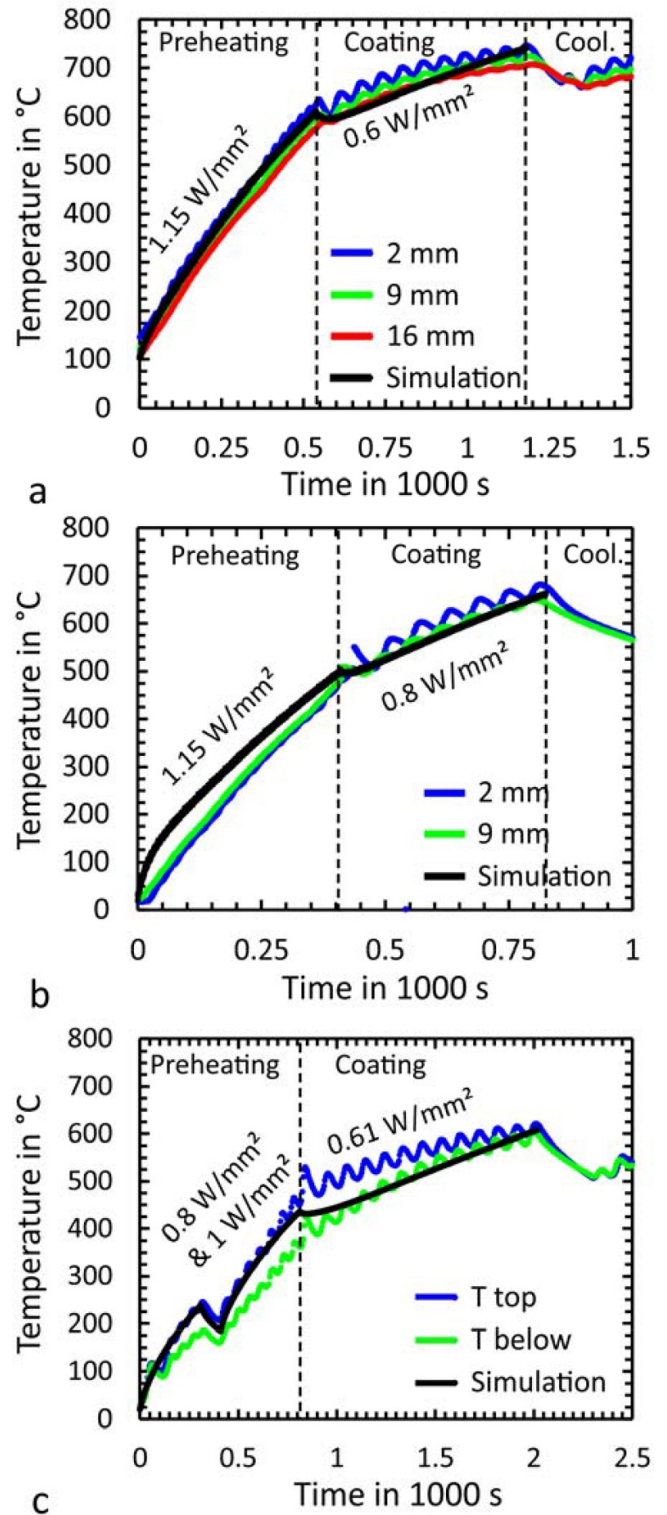
Figure 23. A comparison of temperature trends measured at different distances from the substrate top surface with those simulated for (*a*) the first small test mock-up, (*b*) the second small test mock-up, coated with a lower maximum temperature, and (*c*) the larger mock-up.

restrictions at the free edge. In regard to the fields of von Mises stresses in the range of 340 to 570 MPa, they cover an even larger area than in the previous case.
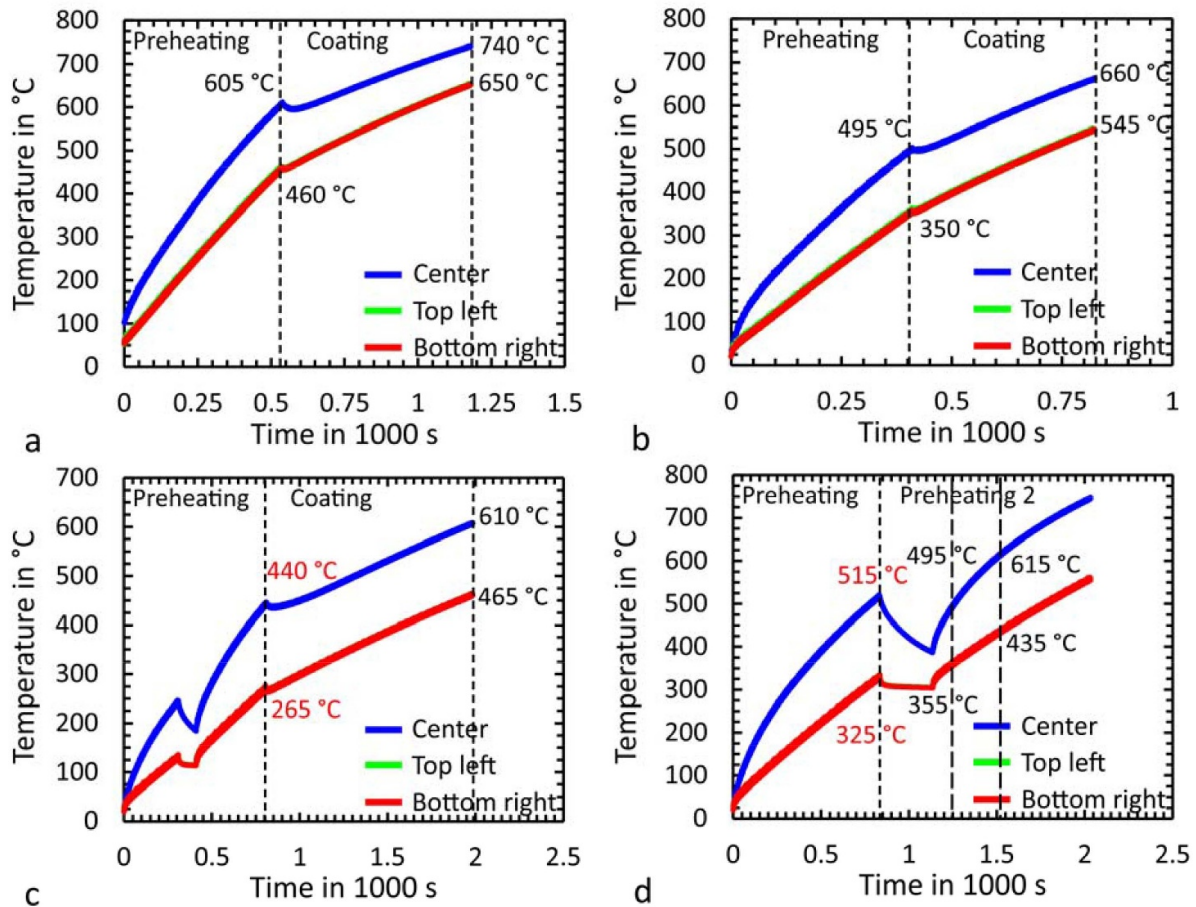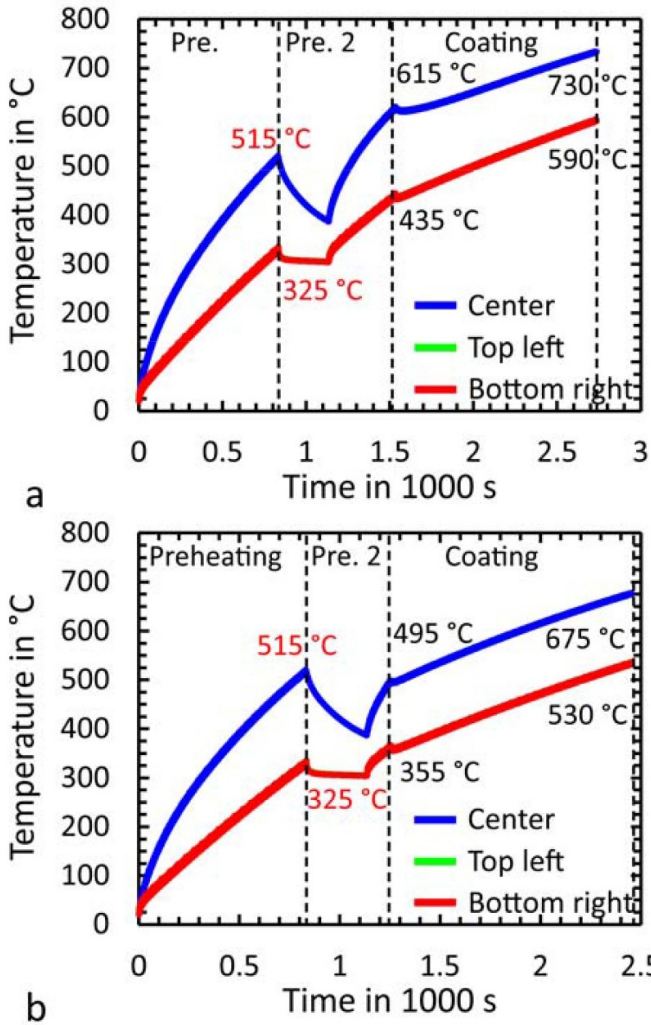
Figure 24. Simulated temperature trends for the center and the corners of the coating area of (*a*) the first small mock-up, (*b*) the second small mock-up, coated at a lower maximum temperature, (*c*) the larger mock-up and (*d*) the larger mock-up with additional preheating.

Another option is to introduce a shoulder by increasing only the width of the FG-layer, whereas the W-layer remains the same (figure 20) thus reducing the load on the FG-coating edge. This approach diminishes the fields with high von Mises stresses observed at the edge region in the previous simulations, and produces significantly lower stresses at the coating edge tip. Hence, the last design modification is chosen for the new coating.

4.2.2. Coating process. In regard to the coating process, the preheating is of particular interest, to achieve the required temperatures for the formation of metallurgical bonding on the whole coating area, and was simulated by heat transfer simulations. The simulations were conducted on simplified models of the mock-ups (figure 21) to which the thermal properties of EUROFER (table 7) are applied. For the three-dimensional geometries tetragonal heat transfer elements were used for convenience. Based on the temperature measurements depicted above, the heat fluxes $\dot{Q}$ from the spraying system were estimated and temperature distributions as well as trends simulated. For the fitting, the temperatures at the upper and lower node of the heat transfer element, which would be close to the thermocouples in the real mock-ups, were compared to the measured ones.

The movement of the cone-shaped spraying plasma was also taken into account in the simulation and its velocity was set to 0.5 m s^{-1}. This was accomplished by first dividing the coating area equally into 45×32.5 mm^2 large fields, which represent the plasma cone area. Each of these fields was then heated by a heat flux that was linearly increased and decreased over time. Figure 22 gives a schematic visualization of the spot movement over the different field and heat flux amplitudes as a function of time. The step duration equals 0.045 s and is calculated, for instance for the smaller mock-up, out of the necessary time of 1.08 s to cover the length of 12×45 mm at a speed of 0.5 m s^{-1} for an assumed number of 24 steps. A short cooling of the components between preheating and coating, due to the short removal of the plasma for introducing the powder, is also possible and was tested in the form of a heat flow from the whole outer surface of the mock-ups. This develops, however, significant discrepancies between the simulated and measured temperature trends, so that such cooling in between was not further considered in the simulations.
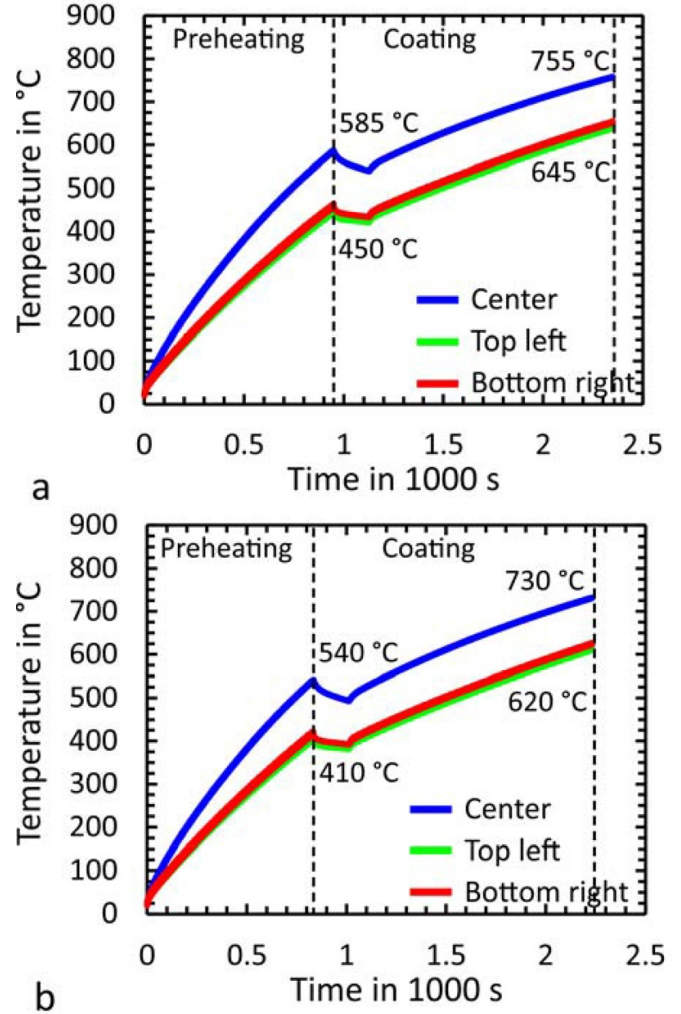
The temperature trends simulated in this way are compared to the measured ones in figure 23, with the corresponding heat flows and fluxes utilized in the different steps of preheating and coating additionally noted in the charts. The oscillations in the measured temperature trends, particularly during coating, reflect the scanning movement of the plasma gun, repetitively

Figure 25. The simulated temperature trends for the center and the corners of the coating area of the larger mock-up starting from an initial coating temperature similar to (*a*) the first small mock-up and (*b*) the second small mock-up, coated with a lower maximum temperature.

Figure 26. Simulated temperature trends for the center and the corners of the enlarged coating area of the larger mock-up starting from an initial coating temperature similar to (*a*) the first small mock-up and (*b*) the second small mock-up, coated at a lower maximum temperature.

approaching and moving away from the position of the measuring thermocouple. In the case of the smaller mock-ups (figures 23(*a*) and (*b*)), the temperatures decrease at the beginning of the coating step, in which a smaller heat flux is used than during preheating. This implies that during the simulation heat had accumulated during preheating in the area of the cooling channels, possibly due to the lower amount of material for heat transfer. This heat accumulation was then able to dissipate under the lower heat flux during the coating and a new equilibrium of heat input and transfer develops. In regard to the larger mock-up (figure 23(*c*)), the temperature slopes are interrupted and change during preheating, because the mock-up was first preheated at a lower power level to observe the behavior, before increasing the power to normal levels.

Based on these simulations the temperatures at the coating area corners can also be approximated from the simulation data. The corners are of special interest, because there the temperatures could be minimal and the layers susceptible to delamination, due to the distance to the coating area center and geometry, respectively.

In the case of the first smaller mock-up (figure 24(*a*)) the temperatures were 605 °C at the center and 460 °C at the corners after preheating, while for the second mock-up (figure 24(*b*)) the corresponding temperatures were 495 °C and 350 °C. In the case of the larger mock-up (figure 24(*c*)), however, the temperatures only amounted to about 440 °C at the center and 265 °C at the corners after preheating, which are apparently too low for the development of sufficient layer adhesion. Therefore, the preheating temperatures, like in the successfully coated second smaller mock-up ($\geqslant$500 °C), are assumed to be the minimal preheating temperature. However, these temperatures are not achieved even if a heat flux of 1 W mm^{-2} is used from the start for the same preheating duration (figure 24(*d*)). Hence, longer preheating is necessary, which will, however, intensify the temperature difference between the center and the corners due to the different temperature increases. To avoid overheating in the center by heat accumulation and achieve a heating of the coating area that is as homogenous as possible, the preheating could be suspended, e.g. for five minutes. This would allow the heat
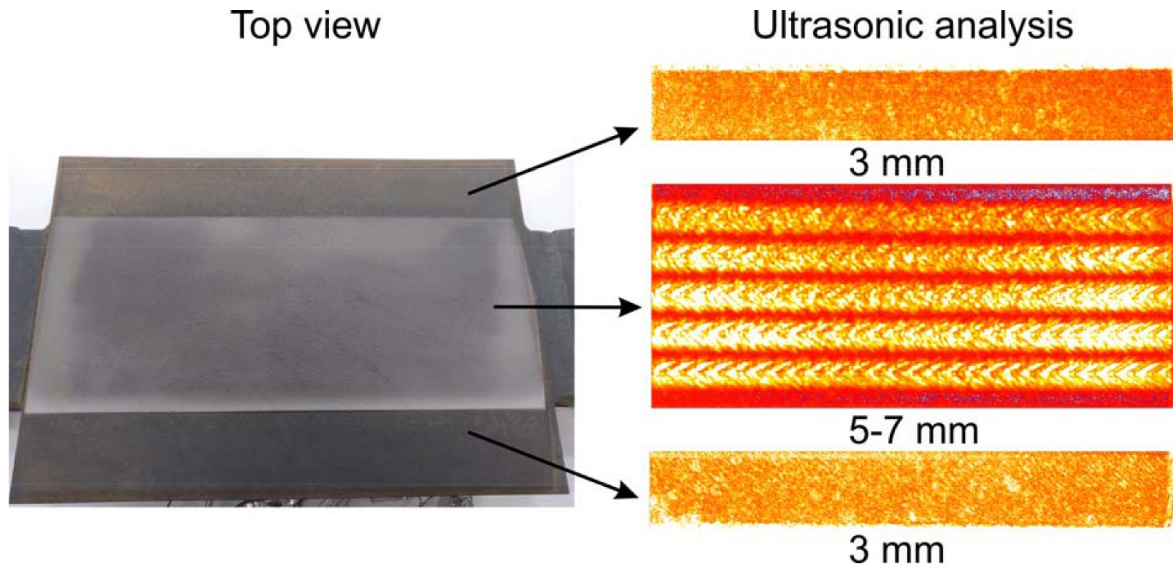
Figure 27. A top view of the larger mock-up with a second coating after ultrasonic testing and the results of the latter with specific analysis depths. The visibility of the cooling channels with the cooling ribs and the homogeneous color pattern of the C-scan images at around 3 mm depth are clear indications that the coating layer above is defect/delamination free.

accumulation to dissipate, so that the temperature difference can be reduced from nearly 200 °C to about 90 °C. During additional preheating, with the same heat flux, it was possible to achieve temperatures like those for the first and second small test mock-ups as marked in figure 24(*d*) by the two vertical dashed lines at ≈1250 s and ≈1500 s, respectively. Proceeding from this preheating with the coating, similar temperatures are also generated after the duration of 1200 s correspondingly to the first and second small mock-up (figure 25).

In view of widening the FG-coating to the whole surface, preheating can also be performed on a larger area. This is reproduced in the thermal analysis by extending the coating area on the model (figure 21) to 270×200 mm^2 and dividing it into 24 fields of 45×50 mm^2. Due to the larger area, a heat flux of 1 W mm^{-2} can be applied to the surface temperatures, like for the second and first smaller mock-ups, already achieved after 835 and 950 s, respectively (figure 26). Therefore, additional preheating is not required. A short break of about 180 s allows the temperature difference between the center and the corners to dissipate from around 130 °C to about 105 °C. Continuing from this point with the coating, the surface reaches temperatures of 755 °C and 645 °C or 730 °C and 620 °C, respectively, after a duration of 1200 s. The higher temperatures of the first trend would be advantageous for developing good layer adhesion [2], though the latter trend was chosen for the new coating of the larger mock-up, due to the limitations of the substrate tempering temperature and the limited heat management of the utilized VPS-facility.

4.3. Coating using optimized coating process

Based on the studies above, a new coating was successfully deposited on the mock-up with a larger FG-coating area, gently inclined slopes and modified preheating. Neither external nor internal adhesion defects were detected, and particularly in the central part, the cooling channels with the cooling ribs are clearly depicted by ultrasonic testing (figure 27).

Figure 28 presents the measured temperature trends during the new coating at the three locations specified in figure 13. The figure emphasizes the effort of the production, as the process has to be interrupted and restarted several times, so that the VPS-facility itself is able to cool down. In contrast to the performed simulations, however, the temperature differences are clearly smaller than 100 °C and often in the range of only about 60 °C, while the temperatures at the perpendicular position are often higher than at the other two locations. The lower temperature discrepancies indicate that the thermal conductivity of the materials is actually larger than the assumed values (table 7), which were extrapolated from data that was experimentally determined only up to about 600 °C [12]. At this point it shall be remarked as a side note that equation (9) [12] already provides larger thermal conductivity values than equation (10) [12]. A higher thermal conductivity correlates, first of all, to the determined substrate hardness profiles of the smaller mock-ups (figure 10), from which it follows that local heat accumulation above the cooling channels did not occur. Secondly, the apparently higher thermal conductivity is also corroborated by the wavelike temperature trends, e.g. figure 23, indicating that heat from the spraying plasma plume dissipates faster than calculated by FE-simulations. The wavelike temperature trends imply further that the heat flux of the sprayed powder was higher than the fitted values. In regard to the comparatively higher temperature at the perpendicular position, the respective measurements could have been influenced by the massive side parts (figure 13), which emit their stored heat.

After the successful coating, the mock-up was inspected in regard to pressure vessel standards and subjected to the
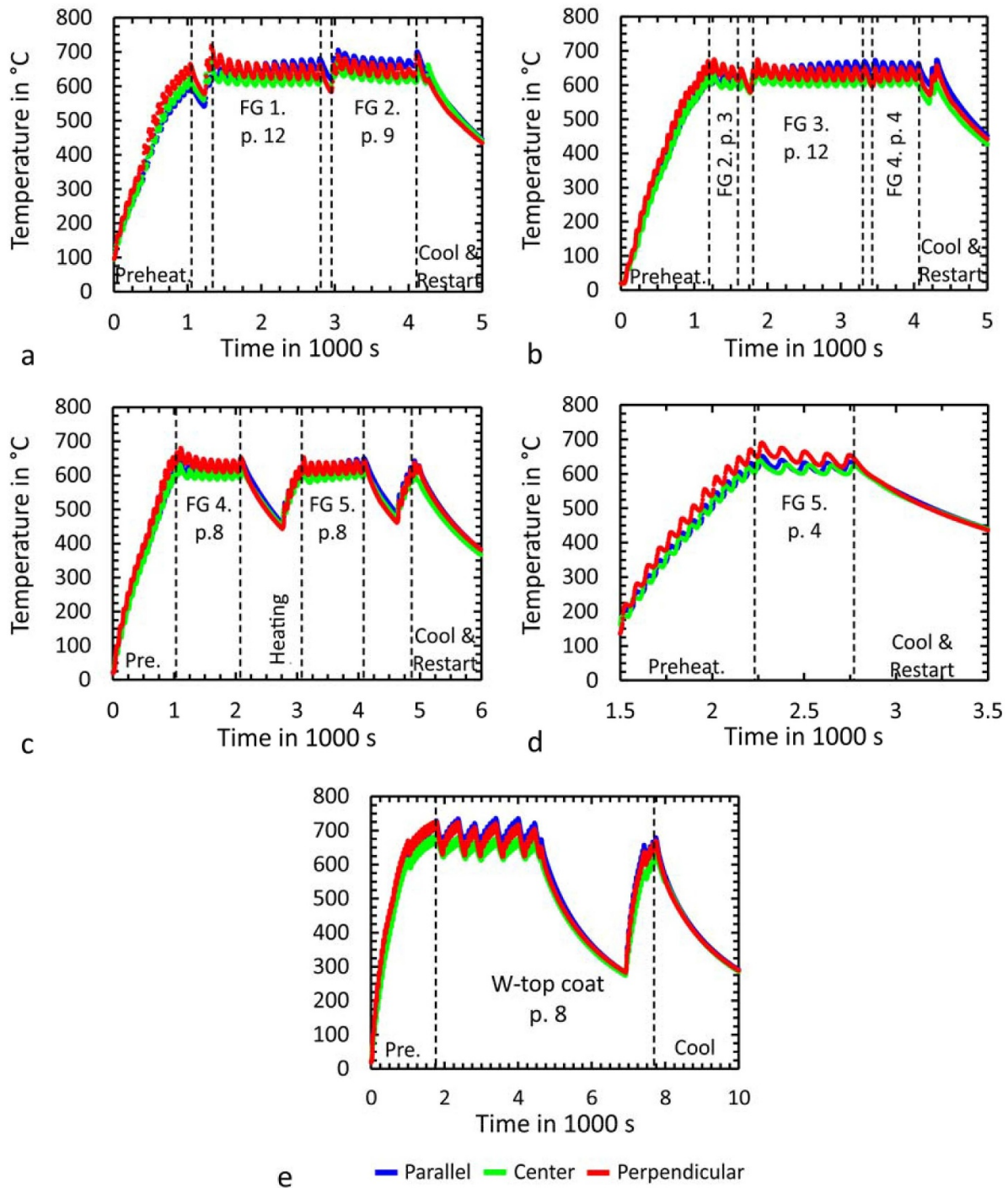
Figure 28. Temperatures in the larger mock-up, at the three locations indicated by figure 13, during preheating, coating and cooling, with the respective number of passes (p.) of the spraying system for depositing (*a*)–(*d*) the FG-layers and (*e*) the W-top coat.

required repair welding, which was performed, based on the gained experience from the previous mock-up, only locally. Subsequently, the mock-up was heat treated in a vacuum furnace for 2 h at 740 °C with furnace cooling to room temperature and no delamination of the coating occurred. Finally, the mock-up was qualified by a conducted pressure test.

In view of previous works to optimize the coating [7], the experiments presented in this work show that significant cooling of the substrate is not a feasible option. It is theoretically attractive, due to lower temperatures and thus lower thermal stress, but sufficient bonding is not achieved on a substrate colder than about 500 °C. For future larger components, active cooling may nevertheless still be an option, to remove the heat from the plasma plume faster at the coating temperature, thus shortening the process time and reducing the thermal load on the facility.

5. Summary and outlook

In this paper the following work on the development of FG W/EUROFER-coatings for a future breeding blanket FW was conducted and promising results gained:

(a) An overview of the thermomechanical material properties was given.
(b) FW mock-ups were manufactured and successfully coated on areas of 270×65 mm^2.
(c) One coated mock-up was successfully tested under fusion-relevant heat loads and helium flows in HELOKA and the durability of the coating system confirmed.
(d) Another larger mock-up was manufactured and successfully coated with the FG layer system on an area of 270×200 mm^2 with a tungsten top coat on an area of 270×115 mm^2, after a process optimization supported by FE-simulations.

For future even larger mock-ups or full scale components, coating on a laboratory scale is no longer possible. Therefore, first development tests for coating on an industrial scale will be carried out. Parallel to this, further durability tests of the coating systems under fusion relevant conditions need to be conducted.

Acknowledgments

ORCID iDs

Thomas Emmerich https://orcid.org/0000-0001-8521-3141
Bradut-Eugen Ghidersa https://orcid.org/0000-0002-7863-6290
Robert Vaßen https://orcid.org/0000-0002-9198-3991

References

[1] Qu D.D., Basuki W.W. and Aktaa J. 2015 Numerical assessment of functionally graded tungsten/EUROFER coating system for First Wall applications *Fusion Eng. Des.* **98–99** 1389–93
[2] Vaßen R., Rauwald K.-H., Guillon O., Aktaa J., Weber T., Back H.C., Qu D. and Gibmeier J. 2018 Vacuum plasma spraying of functionally graded tungsten/EUROFER97 coatings for fusion applications *Fusion Eng. Des.* **133** 148–56
[3] Qu D. 2016 Development of functionally graded tungsten/EUROFER coating systems *PhD Thesis* (Karlsruhe)
[4] Aktaa J. and Qu D.D. 2016 Spraying 2 mm thick coating system and optimising the spray parameters EUROfusion IDM EFDA_D_2MLW4C
[5] Qu D.D., Basuki W.W., Gibmeier J., Vaßen R. and Aktaa J. 2015 Development of functionally graded tungsten/EUROFER coating system for first wall application *Fusion Sci. Technol.* **68** 578–81
[6] Lindau R. *et al* 2005 Present development status of EUROFER and ODS-EUROFER for application in blanket concepts *Fusion Eng. Des.* **75–79** 989–96
[7] Emmerich T., Qu D.D., Vaßen R. and Aktaa J. 2018 Development of W-coating with functionally graded W/EUROFER-layers for protection of first-wall materials *Fusion Eng. Des.* **128** 58–67
[8] Weber T. and Aktaa J. 2011 Numerical assessment of functionally graded tungsten/steel joints for divertor applications *Fusion Eng. Des.* **86** 220–6
[9] Weber T., Stüber M., Ulrich S., Vaßen R., Basuki W.W., Lohmiller J., Sittel W. and Aktaa J. 2013 Functionally graded vacuum plasma sprayed and magnetron sputtered tungsten/EUROFER97 interlayers for joints in helium-cooled divertor components *J. Nucl. Mater.* **436** 29–39
[10] Emmerich T., Vaßen R. and Aktaa J. 2020 Thermal fatigue behavior of functionally graded W/EUROFER-layer systems using a new test apparatus *Fusion Eng. Des.* **154** 111550
[11] Nagasaka T. 2009 Thermophysical properties and microstructure of plasma-sprayed tungsten coating on low activation materials *Fusion Sci. Technol.* **56** 1053–7
[12] Mergia K. and Boukos N. 2008 Structural, thermal, electrical and magnetic properties of Eurofer 97 steel *J. Nucl. Mater.* **373** 1–8
[13] VdTÜV 2009 Warmfester Stahl X10CrWMoVNb9-2; Werkstoff-Nr. 1.4901 Verband der TÜV e.V., Köln
[14] Arbeiter F., Bachmann C., Chen Y., Ilić M., Schwab F., Sieglin B. and Wenninger R. 2016 Thermal-hydraulics of helium cooled First Wall channels and scoping investigations on performance improvement by application of ribs and mixing devices *Fusion Eng. Des.* **109–111** 1123–9
[15] Verein Deutscher Ingenieure (VDI) 2013 *VDI-Wärmeatlas: Mit 320 Tabellen* 11th (Berlin: Springer Vieweg)
[16] Kuznetsov V. 2010 Cr-Fe-W *Refractory Metal Systems* ed W. Martienssen, G. Effenberg and S. Ilyenko (Berlin, Heidelberg: Springer Berlin Heidelberg) pp 150–5
[17] Neuberger H., Rey J., von der Weth A., Hernandez F., Martin T., Zmitko M., Felde A., Niewöhner R. and Krüger F. 2015 Overview on ITER and DEMO blanket fabrication activities of the KIT INR and related frameworks *Fusion Eng. Des.* **96–97** 315–8
[18] Dassault Systèmes Simulia Corp. 2016 ABAQUS